Master in Chemical Engineering

Electrochemical characterization of cell components for proton exchange membrane electrolyzers

A Master's dissertation

of Ana Glória Moutinho Gonçalves

Developed within the course unit of dissertation

held in
DLR / Institute of Engineering Thermodynamics

**Deutsches Zentrum
für Luft- und Raumfahrt**
German Aerospace Center

Supervisor at FEUP: **Prof. Adélio Mendes**

Supervisors at DLR: **Svenja Stiber and Dr. Aldo Gago**

U.PORTO
FEUP **FACULDADE DE ENGENHARIA**
UNIVERSIDADE DO PORTO

Department of Chemical Engineering

July of 2018

Acknowledgments

I would like to thank DLR and the Institute of Engineering Thermodynamics for providing me the opportunity to develop my research. I am very grateful for the trust and support that Professor K. Andreas Friedrich places in FEUP students allowing them to live this experience.

Thank you to all my colleagues in DLR that helped me to achieve my results not only through the analysis of samples but also by giving their advice and patience: Dr. Indro Biswas, Ms. Ina Plock, Ms. Iris Haug and Jörg Bürkle. To the colleagues that made me laugh in lunch breaks and hallways, it was really nice to know Stuttgart with you!

A big thank you to my supervisors in DLR, Dr. Aldo Gago and Svenja Stiber, you gave your knowledge, guidance, time and support and I will never forget how much I grew and learned in this challenging project thanks to you.

To my supervisor at FEUP, Prof. Adélio Mendes, thank you not only for the support but also for the motivation and inspiration to be better and more curious than the day before. I am very grateful for the time that you invested in my work.

A big thank you to Tiago Lagarteira for all the learning and advices. You truly helped me with the first steps on how to tackle this project. I would like to thank Prof. Miguel Madeira and all my professors in FEUP that contributed to my academic path and career in this amazing course.

I am very grateful for the financial support from ERASMUS+ programme and a big thank you to DCoop team in FEUP for helping the students in the abroad experience.

To BEST Porto, my dear student association, that made me *work hard and party harder*, introduced me to a world of opportunities and gave me friends for life. To my dearest friends Beatriz, Catarina, Clara, Garrido, Joana, Jorge, José, Miguel, Tiago and Sofia. I missed you like crazy, thank you for the ride along the years! To David, thank you for being my rock.

To my parents, brother and uncle, for all the sacrifices, guidance, support and always being there when I needed.

Abstract

Energy from renewable sources are in a quest to replace fossil fuels. In Europe it is expected an electricity surplus increasing originated by the seasonality of the energy production from renewable sources, creating a potential market for long-term storage. Hydrogen, when produced by water electrolysis, is one of the most promising energy carrier for the large scale storage of energy, mobility, de-carbonization of refineries and chemistry industries. Proton exchange membrane (PEM) electrolysis is the most suitable technology given its high level of maturity and hydrogen purity, low footprint and wide range of operation. Yet, is still expensive, mainly due to the stack materials and components such as gas diffusion layers (GDL) that are made of titanium coated with precious metals, and therefore compromising 43 % of the costs in a stack. In this regard, stainless steel GDLs would preferable to reduce the stack cost and thus the price of hydrogen produced by PEM electrolysis. However, stainless steel corrodes severely in the acidic environment of the PEM electrolyzer.

In this work, it was investigated the performance and durability of low cost stainless steel GDL meshes coated with porous layers of Ti and Nb by vacuum plasma spraying. Coated and uncoated Ti meshes were used for comparison purposes. The morphology and elemental composition of the GDLs was analyzed by scanning electron microscopy (SEM) and X-ray energy dispersive spectroscopy (EDX), respectively. The high purity Ti and Nb layers covered the substrate uniformly. The electrochemical characterization was carried out in 4 cm^2 active area PEM electrolyzer. The polarization curve showed a reduction in overpotential of *ca.* 320 mV at 2 A·cm^{-2} with the Ti/Nb-coated stainless steel mesh, compared to the uncoated Ti mesh. This result means an improvement efficiency of *ca.* 10 %, which can hardly be achieved with more active anode catalysts and thinner membranes. Electrochemical impedance spectroscopy showed an almost complete elimination of mass transport losses at low and high current densities for all coated GDLs when compared to uncoated ones. Furthermore, a 435 h test at constant current density of 2 A·cm^{-2} was carried out for Ti/Nb-coated stainless steel mesh. The cell potential rapidly increased over time, mainly due to technical difficulties with the electrolyzer setup, which needs to be improved in the future for long-term tests. The deionized water ion exchange resin was analyzed in the end of the test by X-ray photonelectron spectroscopy (XPS) and no traces of iron, chromium or other possible corrosion products from the stainless steel were detected.

The Ti/Nb coatings protected the stainless steel mesh GDLs against corrosion and improved substantially the cell performance at high current densities. These coated GDLs can potentially reduce the capital cost of PEM electrolyzers for large-scale hydrogen production from energy from renewable sources.

Keywords: PEM electrolysis, coatings, cost reduction, gas diffusion layer, MPL.

Sumário

A energia proveniente de combustíveis fósseis tem vindo a ser substituída por energia proveniente de fontes renováveis. Na Europa espera-se um aumento do excedente de eletricidade originado pela sazonalidade da produção de energia a partir de fontes renováveis, criando um mercado para o armazenamento da mesma a longo prazo. O hidrogénio, quando produzido através da eletrólise da água, é um vetor energético promissor com aplicações no armazenamento de energia em larga escala, mobilidade, descarbonização de refinarias e indústrias químicas. A eletrólise *PEM (Proton Exchange Membrane)* é a tecnologia mais adequada dada a sua alta maturidade e pureza de hidrogénio, baixa pegada ecológica e ampla gama de funcionamento. No entanto, esta tecnologia ainda se encontra dispendiosa devido aos materiais e componentes do sistema, tais como as camadas de difusão de gás *(Gas diffusion layer - GDL)* que são feitas de titânio revestido com metais preciosos e, portanto, comprometendo 43 % dos custos no eletrolisador. O uso de aço inoxidável na *GDL* poderia reduzir os custos de um eletrolisador, e, consequentemente reduzir o preço do hidrogénio produzido pela eletrólise *PEM*. No entanto, em meio ácido o aço inoxidável corrói severamente o eletrolisador *PEM*.

Neste trabalho, foi avaliada o desempenho e durabilidade de *GDLs* de malhas de aço inoxidável foram revestidas com camadas porosas de Ti e Nb através da metalização por plasma em vácuo. Para fins de comparação, foram usadas *GDLs* de Ti revestidas e não revestidas. A morfologia e composição elementar das *GDLs* foram analisadas através de microscopia eletrónica de varrimento e espectroscopia de raios X por dispersão em energia, respetivamente. As camadas de Ti e Nb apresentaram alta pureza e cobriram o substrato uniformemente. A caracterização eletroquímica foi realizada em eletrolisadores PEM com uma área ativa de 4 cm^2. A curva de polarização mostrou uma redução no excesso de potencial de quase 320 mV a 2 A·cm^{-2} para a *GDL* de aço inoxidável revestida com Ti/Nb, quando comparada com a *GDL* de Ti não revestida. Estes resultados significam uma melhoria de *ca.* 10 %, que dificilmente poderia ser alcançada usando catalisadores mais ativos no ânodo ou membranas mais finas. A espectroscopia de impedância eletroquímica mostrou uma eliminação quase completa das perdas de transporte de massa a baixas e altas densidades de corrente para todas as *GDLs* revestidas, quando comparadas com as não revestidas. Adicionalmente, foi realizado um teste de 435 h a densidade de corrente constante de 2 A·cm^{-2} para a *GDL* de aço inoxidável revestida com Ti/Nb. O potencial da célula aumentou rapidamente ao longo do tempo, devido a dificuldades técnicas na configuração do eletrolisador, algo que requer ser melhorado no futuro a fim de se realizar testes a longo prazo. Uma resina de permuta iónica foi analisada no final do ensaio por espectroscopia de fotoeletrões excitados por raios X, onde não foi detetado nenhum vestígio de ferro, crómio ou outros possíveis produtos de corrosão do aço inoxidável.

Os revestimentos de Ti/Nb protegeram as *GDLs* de malhas de aço inoxidável contra a corrosão e melhoraram substancialmente o desempenho da célula a altas densidades de corrente. Estas *GDLs* revestidas podem reduzir potencialmente o custo de capital dos eletrolisadores PEM para a produção de hidrogénio em grande escala a partir de energia de fontes renováveis.

Palavras-chave: Eletrólise PEM, revestimentos, redução de custos, camada de difusão de gás.

Declaration

I hereby declare, on my word of honor, that this work is original and that all non-original contributions were properly referenced with source identification.

Sign and date

Ana Glória Martinho Gonçalves
05/07/2018

Table of Contents

Notation and Glossary

Latin Letters

a	Concentration activity	-
E	Electrode potential	V
F	Faraday constant	96485 C·mol^{-1}
G	Gibbs free energy	J
H	Enthalpy	J
I	Current	A
J	Current density	A·cm^{-2}
n	Number of moles of electrons transferred	mol
R	Universal gas constant	J·mol^{-1}·K^{-1}
R	Resistance	Ω
S	Entropy	J·K^{-1}
T	Temperature	K or °C
Z	Impedance	Ω

Greek Letters

Δ	Difference operator	-
ε	Efficiency	%
η	Overpotential	V
φ	Phase angle	°
ω	Angular frequency	rad·s^{-1}

Indexes

´	Real
´´	Imaginary
0	Standard conditions (25°C, 1atm)
a	Activation
bub	Bubbles
diff	Diffusion
g	Gas
l	Liquid
ohm	Ohmic
th	Thermoneutral
r	Reactants

List of Acronyms

AC	Alternating current
AST	Accelerated stress test
BPP	Bipolar plate
CAPEX	Capital expenditure
CCM	Catalyst coated membrane
Ch	Characterization
DI	Deionized water
DLR	Deutsches Zentrum für Luft- und Raumfahrt
EDX	Energy dispersive X-ray spectroscopy
EIS	Electrochemical impedance spectroscopy
EU	European Union
GDE	Gas diffusion electrode
GDL	Gas diffusion layer
GHG	Greenhouse-gas
HER	Hydrogen evolution reaction
HHV	High heating value
ICP-MS	Inductively coupled plasma mass spectrometry
ICR	Interfacial contact resistance
KPI	Key performance indicator
LTM	Long-term measurement
MEA	Membrane electrode assembly
MPL	Macro-porous layer
OER	Oxygen evolution reaction
PC	Pre-characterization
PEM	Proton exchange membrane
PFSA	Perfluorsulfonic acid
PTFE	Polytetrafluroethylene
PTL	Porous transport layers
SEM	Scanning electron microscopy
VPS	Vacuum Plasma Spraying
XPS	X-ray photoelectron spectroscopy

1 Introduction

1.1 Framing of the Work

A dynamic transformation has been happening in the energy sector, since the beginning of the 21st century, to reach a sustainable future for the upcoming generations. The way energy is harvested, used and its life cycle, are now a hot topic in most conventions and agreements between countries. Renewable energy sources are in a quest to replace fossil fuels, where the Paris Agreement of the United Nations Framework Convention on Climate Change, in 2015, was a breakthrough to promote actions to keep global warming below 2 °C [1].

At the European Union (EU), in 2015, fuel combustion activities represented 75.4 % of total greenhouse-gas (GHG) emissions, where 36.9 % was due to energy industries and 26.9 % related to the mobility sector [2]. Consequently, the development of sustainable fuels are seen as the key to achieve the EU goal of having at least 10 % of transport fuels resultant from renewable sources by 2020 [1]. In 2015, Portugal produced 1.6 % of total GHG emissions in the EU and increased 18 % of its emissions compared to 1995 [2]. With this in mind, the Portuguese National Strategic Plan for Energy states that the introduction of fuel cell and hydrogen technologies, the increase of energy efficiency and a decentralized production of energy using renewable sources, must be the next steps forward to achieve the European goals by 2020 [3]. According to **Figure 1,** the Portuguese national net demand has been mostly constant, while the import balance has been decreasing and creating a surplus of available power [4].
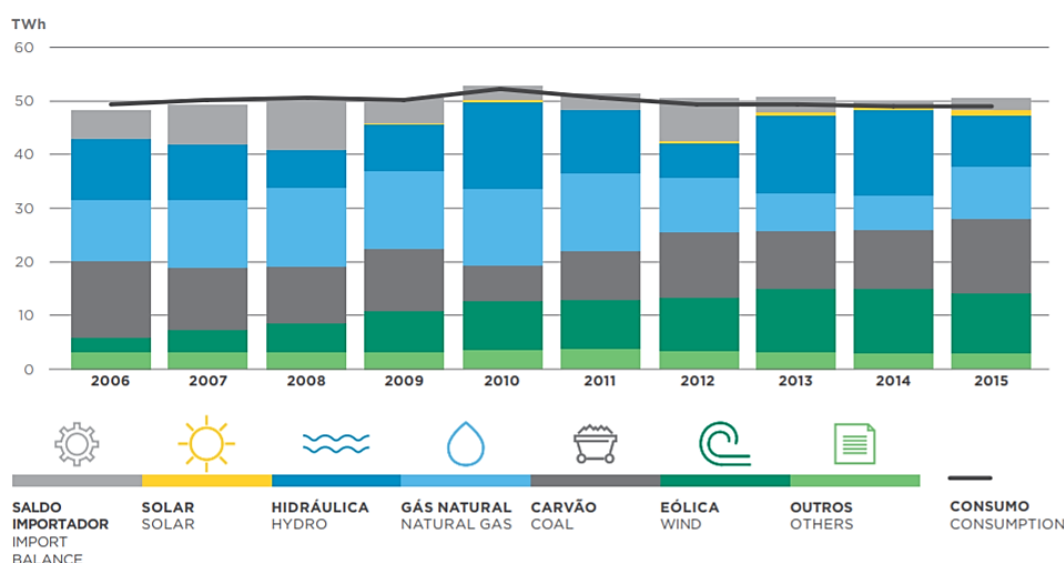

Figure 1 - Portugal data from 2006 till 2015 concerning the supply and consumption of energy in TWh (extracted from [4]).

In Europe, also in Portugal, it is expected an electricity surplus increasing originated by the seasonality of the energy production from renewable sources, creating a potential market for long-term storage [5]. With this in mind, hydrogen becomes an important energy carrier when produced from water electrolysis with the surplus energy as a feedstock. Additionally, helps reducing GHG emissions, since it can be used in the mobility sector.

Hydrogen production has different feedstocks and processes associated to it, from fossil fuels, steam methane reforming, to biomass gasification and water splitting [6]. The global hydrogen demand in 2010 was 43 Mtons and by 2025 it is expected to be *ca.* 50 Mtons [7]. Industry is the largest consumer of hydrogen, representing more than 90 % of its share, followed by the mobility sector [7].

Table 1 shows characteristics between some hydrogen production processes. The hydrogen steam methane reforming is the cheapest and most widely used, even though it needs purification processes afterwards to increase the hydrogen purity.

Table 1 - Some hydrogen production methods and their capacity, efficiency, life time and maturity.

Production method	Capacity	Efficiency (%)	Life time	Maturity
Steam methane reforming [8]	150 – 300 MW	70 – 85	30 years	Mature
Solar methane cracking [9]	5 kW [10]	70	-	Development
Biomass gasification [9]	20 - 450 kW [11]	40 - 50	30 years [8]	Mature
Photocatalytic water splitting [9]	-	10 - 14	-	Development
Water electrolysis [8]	Up to 150 MW	65 - 90	Maximum of 90 000 hours	Mature and in development
High temperature solar steam electrolysis	4 kW [12]	45 [9]	-	Development

The focus of this work is on water electrolysis, since is becoming more competitive as research evolves and shows not only high efficiency but also high hydrogen purity.

Figure 2, shows some possibilities to integrate water electrolysis in the electricity grid. Water (H_2O) and electrical energy are the sources/reactants for this process to take place, where hydrogen (H_2) and oxygen (O_2) are the products. The blue letters represent the different types of systems that uses hydrogen as feedstock. Power-to-power systems re-electrifies hydrogen to be used in a gas turbine or fuel cell, to generate power [8]. Hydrogen can be transformed to methane (when it reacts with CO or CO_2), in a process called methanation and later integrated to the gas grid [8].

For the mobility use, the system is called power-to-fuel. Power-to-feedstock is when hydrogen is used to produce chemicals in the industry sector [8]. Knowing that water electrolysis has an average efficiency of 70 % [8], the efficiency value for the final sector (industry, mobility, power generation or gas grid) is *ca.* 30 % [8] – **Figure 2**, after processes of compression, transport and distribution.
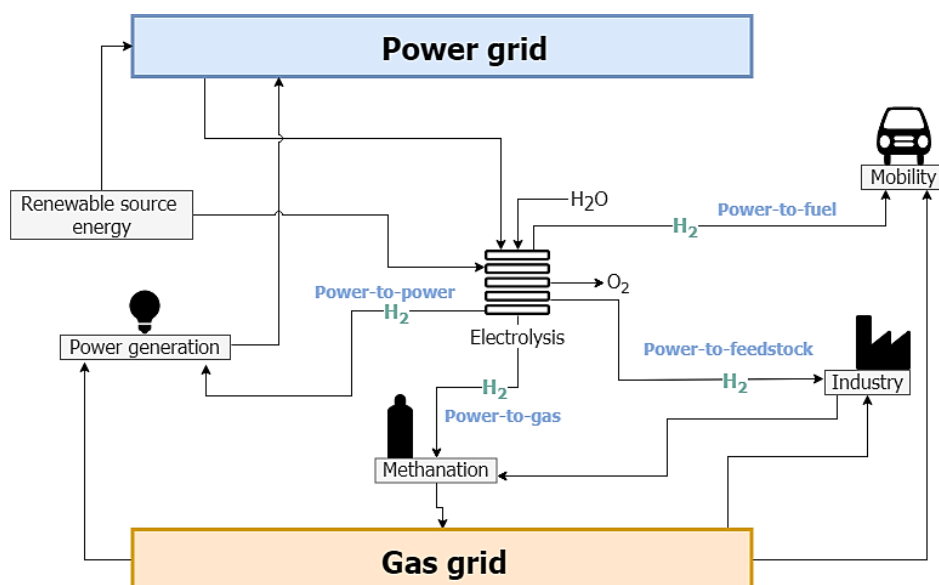

Figure 2 - Potential uses of hydrogen from water electrolysis. In blue letters are the different types of systems that uses hydrogen as a feedstock (based on [1]).

The three main water electrolysis technologies nowadays are: alkaline, proton exchange membrane (PEM) and solid oxide. They differ mostly in their electrolyte and operation temperature [13]. PEM electrolysis is the most reliable hydrogen production process for the transport sector, since it is the only technology that reaches the requirements for high hydrogen purity of 99.995 % [7], even though does not have the same maturity as alkaline electrolysis.

The scope of this work is to investigate the performance and durability of low-cost coated gas diffusion layers in a 4 cm^2 PEM electrolyzer cell.

1.2 Presentation of the Company

The work here presented was done in the Institute of Engineering Thermodynamics of The German Aerospace Center – Deutsches Zentrum für Luft- und Raumfahrt (DLR) - located in Stuttgart. This center has an extensive research and development work in aeronautics, space, energy, transport, security and digitalization. The department of Electrochemical Energy Technology focuses on the development of efficient electrochemical storage and conversion devices, where the Electrolyzer's Team is integrated.

1.3 Contributions to the Work

The reported research contributes for improving the knowledge on the effect of the performance of an electrolyzer cell using a macro-porous layer coated at the gas diffusion layer. The author was responsible for the electrochemical characterization of stainless steel and titanium gas diffusion layers, coated by vacuum plasma spraying with niobium and/or titanium on the anode side; these layers were never reported before. Additionally, the author demonstrated that a high mass transport resistance at GDL can act as a degradation pathway. These results contributed to new data related to PEM electrolysis degradation.

Concerning the test bench, the author optimized it to allow long-term measurements with a constant potential input; this was achieved using a power supply without remote sense.

For the electrochemical measurements, the author was responsible to perform all the polarization curves and EIS measurements and to choose the most adequate impedance parameters in the impedance device. The electrochemical results and the performance of the electrolyzer were analyzed by the author.

The author assisted to improve a $4\,cm^2$ electrolyzer cell. The author also contributed for clarifying topics on the PEM electrolyzer assembly in a meeting with potential partners of DLR.

All scanning electron microscopy and energy dispersive X-ray images were performed by Ms. Ina Plock, while the X-ray photoelectron spectroscopy measurements were performed by Ms. Iris Haug and Dr. Indro Biswas.

1.4 Organization of the Thesis

The thesis is organized in 6 chapters where the topics are the following:

1. Introduction: framing of the work and presentation of the company;
2. Context and state of the art: brief description of the technology, methods of production on the components and characterization tools used;
3. Materials and methods: description of the materials and methods used in the development of the thesis;
4. Results and discussion: presentation of the results and their discussion;
5. Conclusion: reviewing on the difficulties encountered and a summary of the advantages of the developed work;
6. Assessment of the work done: discussion on the achievement of the goals and observations on the future work.

2 Context and State of the Art

2.1 Fundamentals of PEM Electrolysis

Water splitting is a chemical process where water is split into hydrogen and oxygen molecules, through the use of an external source of energy that can be thermal and/or electrical. When this source is electrical energy, the technology is called water electrolysis and takes place at an electrolyzer. The overall reaction of this technology is as follows:

$$H_2O_{(l)} \xrightarrow{\Delta H_r} \frac{1}{2}O_{2\,(g)} + H_{2\,(g)} \tag{1}$$

The reaction enthalpy denoted above as ΔH_r, represents the amount of energy required to break the water chemical bondings. The electrons (e^-) and protons (H^+) are represented in the half equations below, and the sum of **Equation (2)**, water splitting, with **Equation (3),** hydrogen reduction, equals **Equation (1).**

$$H_2O_{(l)} \rightarrow \frac{1}{2}O_{2\,(g)} + 2H^+ + 2e^- \tag{2}$$

$$2H^+ + 2e^- \rightarrow H_{2\,(g)} \tag{3}$$

The working principle of PEM electrolysis is illustrated in **Figure 3**. The power supply drives **Equation (1)** by applying a current. In acid medium, in the anode side, oxygen is evolved while protons are produced, according to **Equation (2).** Protons migrate, due to the influence of an electric field, to the cathode side where they are reduced, forming hydrogen according to **Equation (3)** [14].
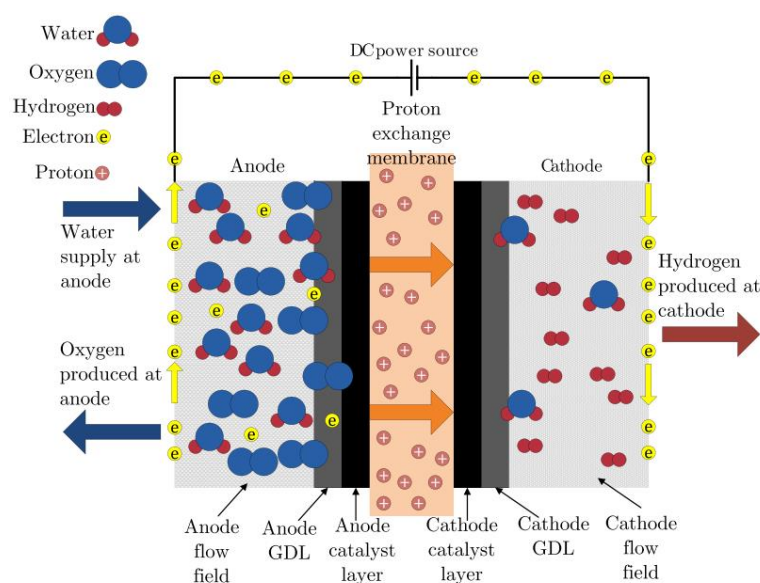

Figure 3 - Diagram of a PEM electrolyzer working principle (extracted from [14]).

The electrochemical cell is divided in two half-cells where a PEM is used as the separator between them. Each half-cell consists in a bipolar plate (BPP), gas diffusion layer (GDL), and an electrode.

To PEM electrolyzers become cost-effective, it is essential that production and investment costs decreases, while the source of energy derives from renewable sources. Presently, the research and development on this technology lays mainly on the catalyst, cell and stack assembly for higher efficiencies [14], while adsorption materials and gas separation membranes focuses on the purification of hydrogen [15]. Although the research on these areas are advanced, questions about durability, degradation and availability of precious metals used for catalyst are still to be answered [16].

Figure 4 shows the cost contribution of each cell component of a PEM electrolyzer, where the stack cost is by far the most important contributing with *ca.* 60 % for the final value [17].
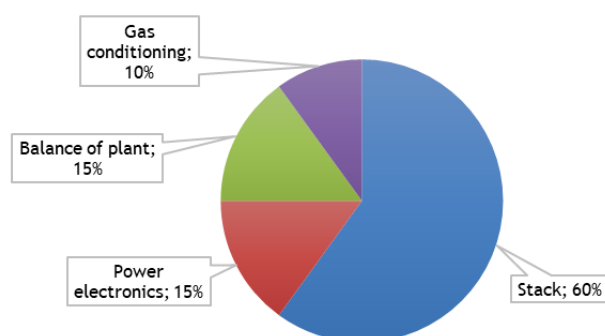

Figure 4 – General costs in a PEM electrolyzer system (based on [17]).

The stack consists of an association in series of electrochemical cells. In the case of BPP having a flow field channel integrated, their cost takes 51 % of the total stack costs [17] – **Figure 5.**
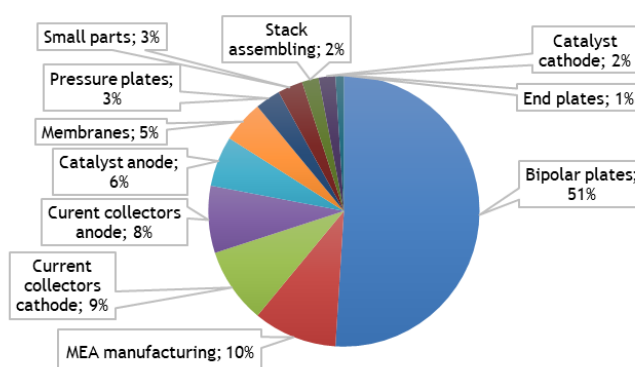

Figure 5 – Costs of a stack in a PEM electrolyzer system with BPP with flow field (based on [17]).

On the other hand, if the flow field is not integrated in the BPP, then this last one is only responsible for 6 % of the costs in a stack [18]. In this case, the highest slice goes to the current collector of the anode side and MEA manufacturing [18], as illustrated in **Figure 6.** Nowadays, the research priority is to reduce the cost the current collectors by developing new materials.
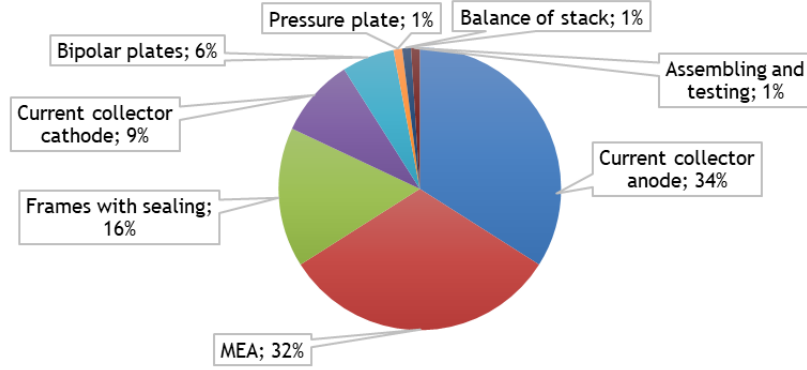

Figure 6 - Costs of a stack in a PEM electrolyzer system with BPP without flow field (based on [18]).

2.1.1 Thermodynamics

As mentioned before, water electrolysis requires an amount of energy to dissociate the water molecule, corresponding to the enthalpy of formation of water, ΔH, described by the following equation:

$$\Delta H = \Delta G + T \times \Delta S \tag{4}$$

The entropy is represented by ΔS and Gibbs free energy, ΔG, represents the maximum reversible work in a system. The potential difference between the anode and the cathode is called the reversible cell potential, E^0, and represents the minimum electrical work required for electrolysis to occur, as seen in **Equation (5)** [13]**.**

$$E^0 = \frac{\Delta G}{n \times F} = 1.229 \text{ V} \tag{5}$$

The number of moles of electrons transferred, n, is two and the Faraday constant, F, is 96 485 C·mol^{-1}, therefore E takes the value of 1.229 V at standard temperature and pressure [13]. Additionally, it is required thermal energy, represented in **Equation (4)** by $T \times \Delta S$, which takes the form of a thermoneutral potential, E_{th}, in the following equation at standard conditions [19]:

$$E_{\text{th}}^0 = \frac{T \times \Delta S}{n \times F} = 0.25 \text{ V} \tag{6}$$

Summing **Equation (5)** with (**6**), a PEM electrolyzer cell should operate with 100 % energy efficiency at 1.481 V. Since enthalpy and Gibbs free energy varies with pressure and reactants activity [20], the reversible cell potential can be calculated by Nernst equation:

$$E = E^0 + \frac{RT}{nF} \times \ln\left(\frac{P_{H_2} P_{O_2}^{1/2}}{P_{H_2O}}\right) \tag{7}$$

Figure 7 represents the heat demand, electrical energy demand and the total energy in comparison to temperature, Nernst potential and energy. PEM electrolysis research and development states that the cell operates below the boiling point of water [13]. With that in mind, in the region below 373.15 K (100 °C) is possible to observe that the thermal energy demanded is less compared to the electrical energy, while the total energy decreases with the increasing of temperature.
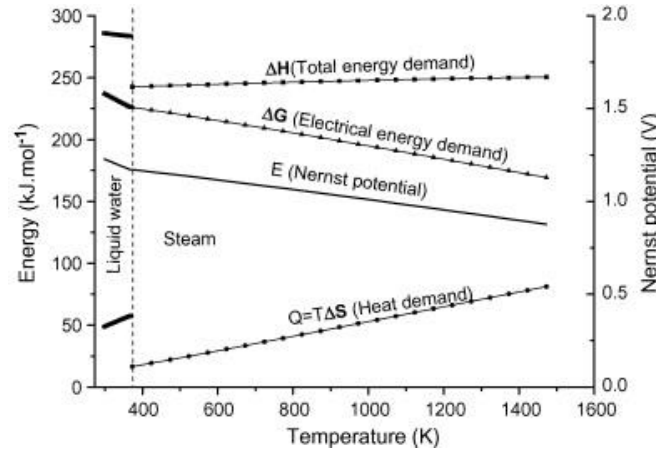

Figure 7 - Enthalpy of reaction vs Temperature vs Nernst potential in water electrolysis (extracted from [21]).

2.1.2 Kinetic Losses

As any other chemical process, losses need to be considered. In PEM electrolysis, the three major contributions for the decrease of the real potential are [22]:

1. Ohmic losses, η_{ohm}: related not only to the resistance from the flow of electrons through the GDL and electrodes, but also to the conduction of protons through the PEM;
2. Activation losses, η_a: associated to the electrochemical reactions at the anode and cathode;
3. Mass transport losses: as a result of the morphology of BPP and GDL, blockage of pores in the GDL from the gas bubbles (η_{bub}), diffusion and convection mechanisms (η_{diff}) [23].

The sum of all these losses, also called overpotentials, with the reversible cell potential gives us the real cell potential, expressed in **Equation (8)** [22]:

$$E_{\text{cell}} = E + \eta_{\text{a}} + \eta_{\text{ohm}} + \eta_{\text{diff}} + \eta_{\text{bub}} \qquad (8)$$

2.1.3 Activation Energy

Activation energy, E_{a}, is the minimum amount of energy to apply for the electrochemical reaction to initiate. It is calculated by difference between the maximum energy value and the energy from the reactants. **Figure 8** illustrates the relation between the activation energy, Gibbs free energy and the reaction history during the electrolysis process, which is an endothermic reaction. In this case, the final products have higher energy than the reactants and the maximum value for energy represents the activated complex. The use of catalysts reduces the activation energy, since it lowers the energy level of the activated complex [24], reducing the Gibbs free energy and therefore increasing the reaction kinetics.
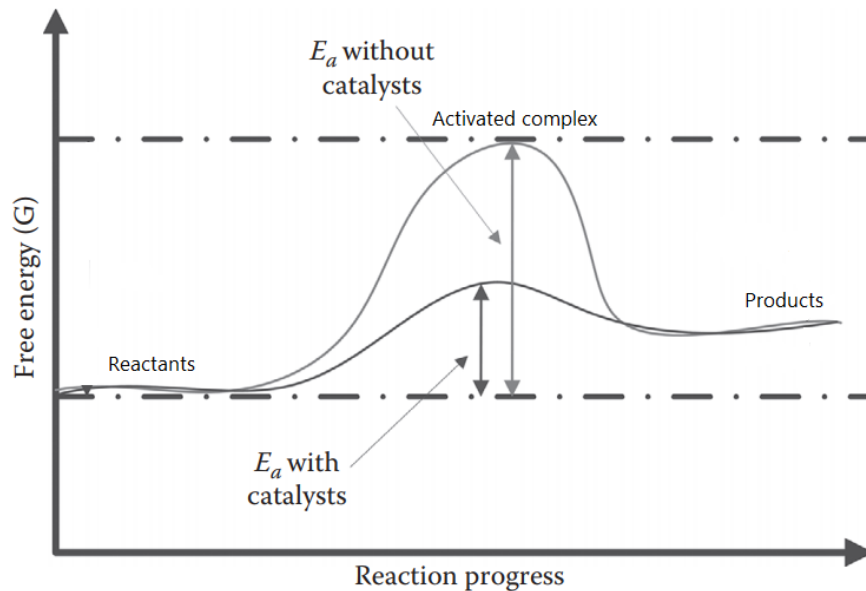

Figure 8 – Relation between the activation energy (E_{a}), Gibbs free energy (G) and the reaction progress over time in an endothermic reaction (based on [13]).

2.2 Main Components of a PEM Electrolyzer

2.2.1 Membrane Electrode Assembly

The MEA (membrane electrode assembly) consists of a PEM and catalysts placed between the two half-cells. The most commonly used PEM in electrolysis is Nafion®, a perfluorsulfonic acid (PFSA)/polytetrafluroethylene (PTFE) based solid membrane [25] that converts the medium acidic. Nafion® is known by its chemical stability and high proton conductivity, although its high cost, difficulties in mechanical stability and decrease in performance while operating at high pressure and temperature are a main focus in research nowadays [25].

The catalysts can be placed on the PEM where this combination is called catalyst coated membrane (CCM), or in the GDL and then having the designation of gas diffusion electrode (GDE) [26]. The anode and cathode side of the MEA corresponds to the side where its corresponding catalysts are coated. These catalysts are normally expensive noble materials, such as palladium or platinum at the cathode, and iridium or ruthenium oxides at the anode [27]. These last ones need to be highly resistant to high potentials (> 2 V) since on the anode the most aggressive reaction occurs, the oxidation of water. Since the reaction only occurs in specific regions of the membrane, called triple-phase boundaries, an Nafion® ionomer is added to increase the contact between the catalysts and Nafion® [26].

The MEA is susceptible to be contaminated and degraded by the metallic ions present in stainless steel, such as Fe, Ni and Cr ions, since this material can be both the GDL and BPP, but also with the ions present in the water. Therefore, it is necessary to use deionized water (DI) to improve the performance of the MEA, together with an ion exchange resin that traps any other ions from the process itself, since those metallic ions will decrease the ionic conductivity [28].

2.2.2 Gas Diffusion Layers

The GDL, also called porous transport layers (PTL) [29], is a porous component placed between the BPP and the MEA, in both half-cells and they are the may focus of this research. Their function is to conduct electrons from the catalytic layer to the BPP, while transporting water to the active area and removing the evolved hydrogen and oxygen. Therefore, in the case of the anode side, they must fulfill a certain number of requirements [30]. The GDLs must be:

1. Porous, with appropriate pore size, pore distribution and porosity;
2. Mechanically stable;
3. Corrosion resistant at cell potentials above 2 V in acid environment;
4. Electrically conductive, *i.e.* having a low contact resistance with the BPP;
5. Low cost.

This last one is nowadays the most important requirement, since the aim is to reduce the CAPEX of electrolyzers. On the cathode side, the state-of-the art is carbon paper or cloth since these materials can endure the reaction of hydrogen reduction, which is not as corrosive as the one in the anode side [29].

Since 2005 several studies have been published on new and improving materials for the anode side. Tanaka *et al.* (2005) published a study on three different types of GDLs, mesh, parallel and crossbar, where the mesh type showed higher uniform electrical conduction than the other two types [31]. The meshes are made from an expanded material that is flat, and afterwards is added a metallic stack tissue [32]. These materials can have different number of lines of tissue per area, different wire diameters and pore sizes [33].

Grigoriev *et al.* (2009) prepared another type of GDLs from powder particles by thermal sintering and studied the relation between pore size and the cell potential [20]. It was concluded that between 50 and 75 microns is the optimum particle size. Additionally, Grigoriev *et al.* wrote that if the particles do not present an appropriate pore size, then the pressure in the catalytic layer increases and therefore affecting the kinetics of the reaction.

Between 2011 and 2013 was published a set of relevant articles by Ito on electrolyzers and by Hwang on fuel cell [34], proposing the use of titanium felts as a good option for the GDL. This GDL is prepared by distributing titanium fibers and then sintered them by thermal processes [35]. Ito *et al.* (2012, 2013) investigated the relation between the fiber diameters, porosity and cell performance, concluding that larger average pore sizes increase the transport of gas and water. However, larger pores can also be detrimental if long slugs are formed within the pore [36], [37].

In industrial large area PEM electrolyzer stacks, the most used materials are meshes and felts, since they are the cheapest GDLs in the market. In the literature, sintered titanium is the material showing better performances in acidic medium and high potentials with minimum corrosion [35], while showing good electrical conductivity. However, it is highly costly. **Figure 9** shows scanning electron microscopy (SEM) images of state-of-art materials for PEM electrolysis [30], such as sintered discs, foams, felts and expanded meshes.
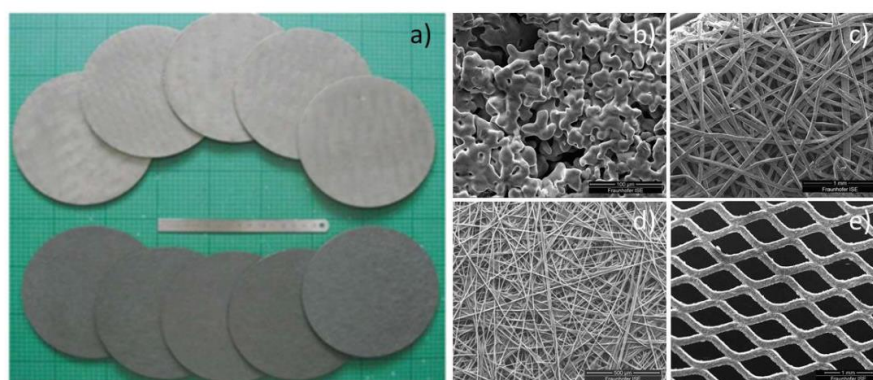

Figure 9 - Examples on materials for the anode GDL in a PEM electrolyzer: a) discs, b) sintered titanium, c) titanium felt, d) carbon, e) mesh (extracted from [30]).

Titanium surface naturally oxidizes to titanium dioxide, in a process called passivation, creating an interfacial contact resistance (ICR), consequently reducing the electric conductivity [35]. Hence, sintered titanium GDLs are often coated with expensive precious metals with properties that show high conductivity [35], therefore reducing the ICR.

Recently, Lettenmeier *et al.* (2016) reported GDLs coated with a titanium macro-porous layers (MPL) [38]. Ohmic losses of the coated GDLs were lower compared to the uncoated ones, together with higher cell performance, since the electrical contact between the components was improved and gaps between the catalyst and the contact layer were reduced [38].

Figure 10 a) and **b)** shows a scheme of sintered titanium coated GDL and its corresponding SEM image, respectively. Small porosity layers are in contact with the catalytic layer, while large pore layers are in contact with the BPP. This pore gradient ensures an efficient release of oxygen gas from the active area.
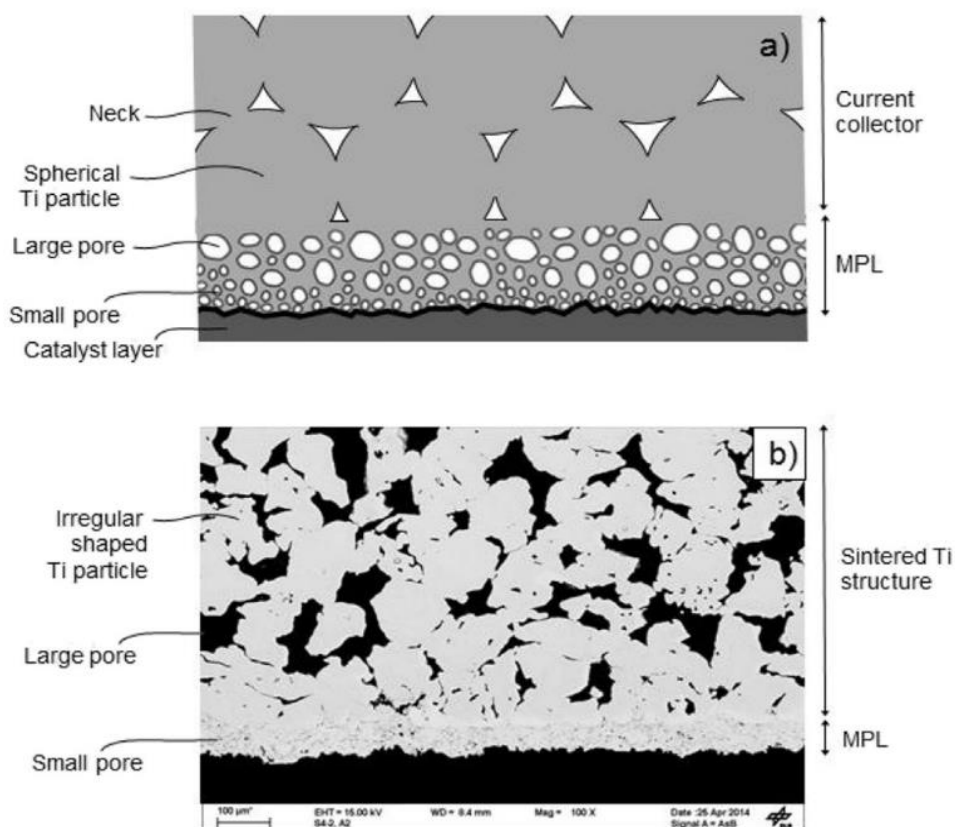

Figure 10 – a) Illustration on the different pore sizes between the MPL and the GDL (represented as current collector), b) SEM image of sintered titanium with a MPL in contact with the catalytic layer (extracted from [38]).

Production Method of Coated GDLs

The MPL can be sprayed in GDLs made of sintered powder or meshes by thermal processes like conventional flame spray, electric arc wire spray, plasma spray and high velocity oxy-fuel spray [39]. The difference between these process relays on its thermal and kinetic energy of the sprayed particles. For GDLs made from metal powders the most suitable thermal process is the plasma spray, since metal has a high melting point. This process can be at atmospheric pressure or in vacuum.

Vacuum Plasma Spraying (VPS) is the process used in this work since vacuum prevents the oxidation of titanium and stainless steel substrate. VPS is a thermal spraying process where molten particles with sizes between 10 and 100 μm [40] are propelled by process gases and sprayed onto a substrate where it solidifies and forms a layer [39]. The principle of this technique is based on a gas which flows between the anode and cathode where it gets ionized, and as a result, a plasma torch develops [39]. The temperature on this plume can reach 15 700 ℃ [39]. On **Figure 11** is represented a scheme of this thermal process.
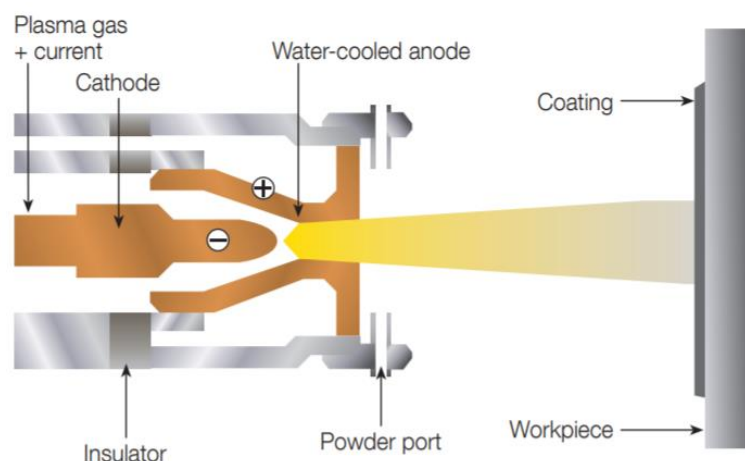

Figure 11 – Illustration of vacuum plasma spraying (extracted from [39]).

This technique is used for coatings of solid oxide fuel cell and electrolyzers components, for electrodes for alkaline electrolysis, and coatings on BPP and GDLs for PEM electrolyzers [30]. The coatings derived from this technique have great quality and reliability, and its proprieties such as thickness, porosity and pore size can be controlled. Therefore, parameters like capillary pressure, bubble point and tortuosity can be analyzed [30].

Physical Characterization of GDLs

To have an insight on the structure of the GDL surface, various techniques from materials science can be used. Electron microscopy is the most used and suitable technique to map the surface of a sample and it uses photons, electrons or ions to generate signals with the surface data.

The instrument available for this work was the scanning electron microscope, with an energy dispersive X-ray (EDX) detector, where it produces images of a sample in order to examine its microstructure morphology, crystalline structure and chemical composition [41]. An electron beam is injected into the sample and collides with an atom, and as a result, the electron beam produces a region of excitation and generates several signals that contains information about the surface [41]. **Figure 12** shows which information is associated to the respective signal.
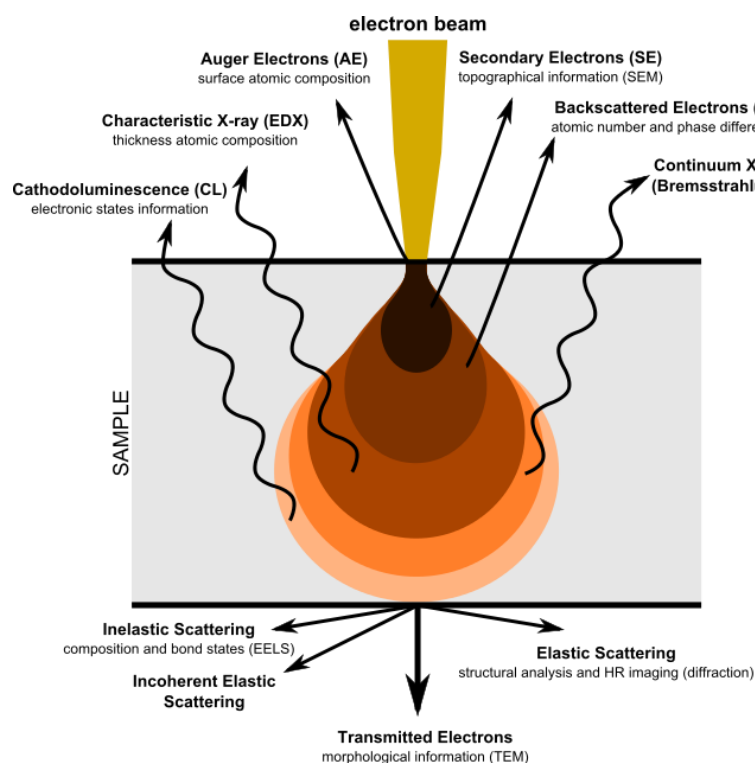

Figure 12 – Illustration on the different signals generated in SEM and its information (extracted from [42]).

This characterization method it is considered to be non-destructive, since the volume of the sample is not lost. Therefore giving the possibility to analyze repeatedly the same sample [43].

2.2.3 Bipolar Plates

A PEM electrolyzer cell has bipolar plates (BPP) enclosing the MEA/GDLs. In most cases, a flow field is integrated in the surface of the BPP with the purpose to transport the formed gases of the reaction while serving as the channel for the water feed entering the GDL [29]. If the flow field is not present in the BPP, then the GDL needs to overtake the function of the flow field.

Similar to GDLs, the anode side needs to be handled with caution since it is where the corrosion takes place. Some of the requirements for a BPP are stable mechanical integrity [44] as well as good electrical and thermal conductivity [30]. The BPP on the anode side should withstand against the acidic corrosion environment. For systems operating at high pressures the BPP from the cathode side also should resist to hydrogen embrittlement and oxidation.

The state-of-art material on the anode side is titanium because endures the corrosion environment [45]. Similar to what happens in GDLs, the passivation of titanium increases the ICR between the GDL and BPP [45]. To diminish this effect, developments have been made on coating BPP with gold and platinum [45]. Although this method decreases the ICR, the process itself is expensive, as a result, developments from Lettenmeier *et al.* (2017) states that BPP of stainless steel could be used as an alternative to titanium [46].

Stainless steel is cheaper and easier to machine than titanium, even though it releases ions, such as Cr, that could poison the MEA. Lettenmeier *et al.* (2017) showed that stainless steel BPP in the anode side had good performance when coated, not only with titanium to prevent corrosion, but also with niobium to prevent the passivation of titanium [45]. Therefore, diminishing the releasing of poison ions into the solution.

The article from Lettenmeier *et al.* (2016) suggested that stainless steel on the cathode side might not require any coating since it showed good performance while resisting to hydrogen embrittlement [28].

2.3 Electrochemical Characterization

2.3.1 Polarization Curve

A typical polarization curve of a PEM electrolyzer is illustrated in **Figure 13**, where all the overpotentials mentioned in **2.1.2** are represented in a cell potential versus current density. The polarization curve is obtained by applying current and cell potential is measured. The source of the input current can be a potentiostat, where the potential is measured automatically, or can be from a power supply and the potential is measured manually with a multimeter or with another relevant appliance. In any case, for a PEM electrolyzer all measurements should be terminated when the cell potential reach 2.4 V. It is necessary to wait for the potential values to stabilize, either with a time step in a manually mode or with a scanning rate with automatic mode, for correctly reading the potential values.
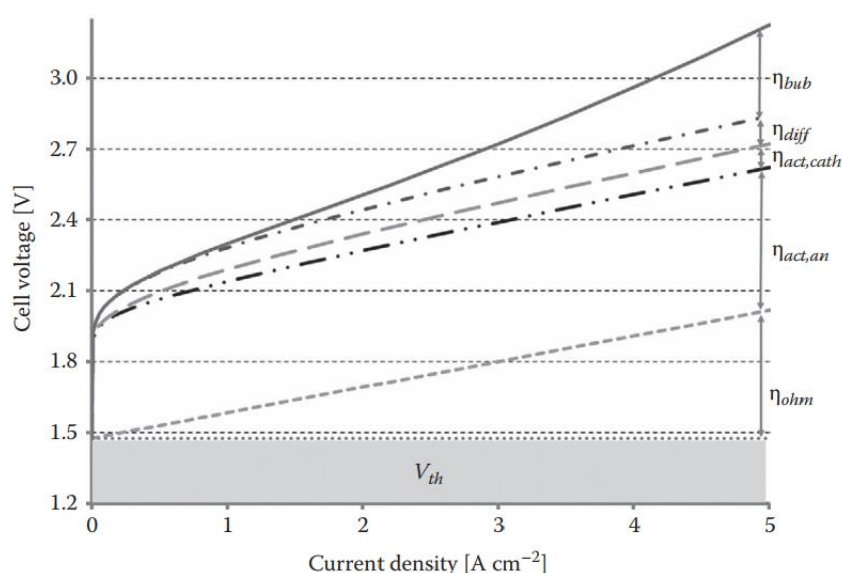

Figure 13 – Polarization curve and overpotentials in a PEM electrolysis cell. η_{act} are the activation losses in the cathode (cath) and anode (an), η_{ohm} are the ohmic losses, η_{bub} and η_{diff} are related to the mass transport losses through the existence of bubbles or diffusion mechanisms, respectively (extracted from [13]).

A polarization curve can give information not only on the major contributions for the decrease of the real potential, but also in changes concerning the operating conditions. Fluctuations on the cell potential could result from variations in the temperature, humidity, pressure and flow rates in the system. At low current densities the activation losses are the major contributions for the potential decrease, the ohmic losses prevail at moderate current densities and at high current densities is the mass transport losses that are more prominent. The linearity of the curve can also give information about the losses in the cell, since an exponential behavior is related to mass transport losses.

Furthermore, a polarization curve is a useful and standard tool to compare the performance between electrolyzers. Probably the most important key performance indicators [47] of an electrolyzer cell is the current density versus the cell potential below, where the highest current density at the lowest cell potential is desirable.

2.3.2 Electrochemical Impedance Spectroscopy

Electrochemical impedance spectroscopy (EIS) is a characterization technique that measures not only the ability of a circuit to resist the flow of current, but also its ability to store electrical energy [48]. This resistance is called impedance, represented as Z_ω in **Equation (9),** and is the ratio between the potential and current in a dynamic system for each frequency [22].

This equation is also related to Ohm's Law at limit of zero frequency for steady-state systems.

$$Z_\omega = \frac{V_\omega}{I_\omega} \tag{9}$$

A EIS device applies a sinusoidal signal potential or alternating current (AC) to the circuit in a specific frequency and the response is measured and plotted in a graph [48], [49], as can be seen in **Figure 14.** This procedure is repeated in a range of frequencies and represented in a Bode or Nyquist graph. In the first one, the phase (φ) is the system response and is plotted as a function of frequency, represented by **Equation (10)** in polar coordinates, with ω being the angular frequency [22]. On the other hand, the Nyquist graph has an imaginary part ($-Z''_\omega$) of the impedance in function of its real part (Z'_ω) at each frequency [49], as seen in **Equation (11)** in cartesian coordinates [50]. In Nyquist graph the highest frequencies are in the area of lowest values of resistance and they decrease while the resistance values increase.

$$Z_\omega = |Z_\omega|e^{\omega\varphi} \tag{10}$$

$$Z_\omega = Z'_\omega - j \times Z''_\omega \tag{11}$$

If the EIS device is measuring the current response of the circuit while giving an input signal of the potential, then is working in potentiostatic mode. On the contrary, if the response is the potential while the current is the input signal, then the EIS device is working in galvanostatic mode.
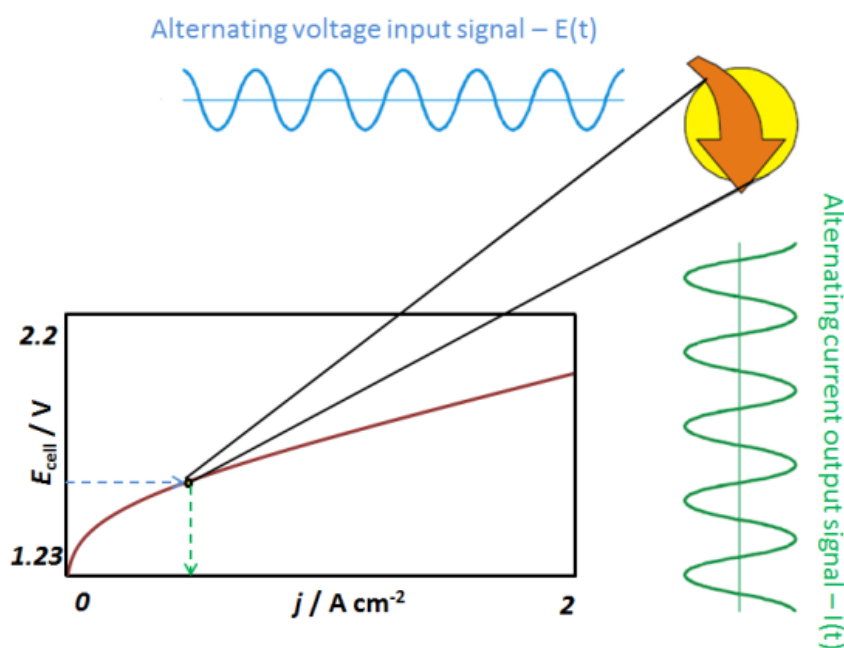
Figure 14 – Schematic representation of the input and output signal in an electrolyzer and their relation in a polarization curve (extracted from [51]).

This electrochemical technique is widely used in the study of catalytic reaction kinetics, diffusion of ions, corrosion, as well as in fuel cells, batteries and electrolyzers [50]. One of the greatest advantages in using EIS is the easy access to the circuit/cell internal information on degradation and performance while the system is working, instead of analyzing post-mortem data [48].

Equivalent Circuit Modeling

It is possible to fit a model to the EIS spectrum and obtaining quantitative parameters that characterize the electrochemical system. This model is represented as an electric analogue and comprehends elements such as resistances, capacitances and impedances, combined in series and in parallel.

Figure 15 shows an example of an equivalent circuit used form modeling the EIS spectrum of a PEM electrolyzer. Concerning the Nyquist plot, recent developments by Lettenmeier *et al*. (2016) showed that the blue arc in the high frequency range - **Figure 15 -** is attributed either to the hydrogen evolution reaction (HER), charge transfer resistance, double layer effects in the electrode or the first charge transfer in the oxygen evolution reaction (OER) [16]. The ohmic resistance is represented by the gray arc, while the red and green arcs, well known and studied in fuel cell systems, are representative of the activation and mass transport losses, respectively [23]. The red and gray arc are related to the high frequency range, while the green arc is related to the low frequency range.
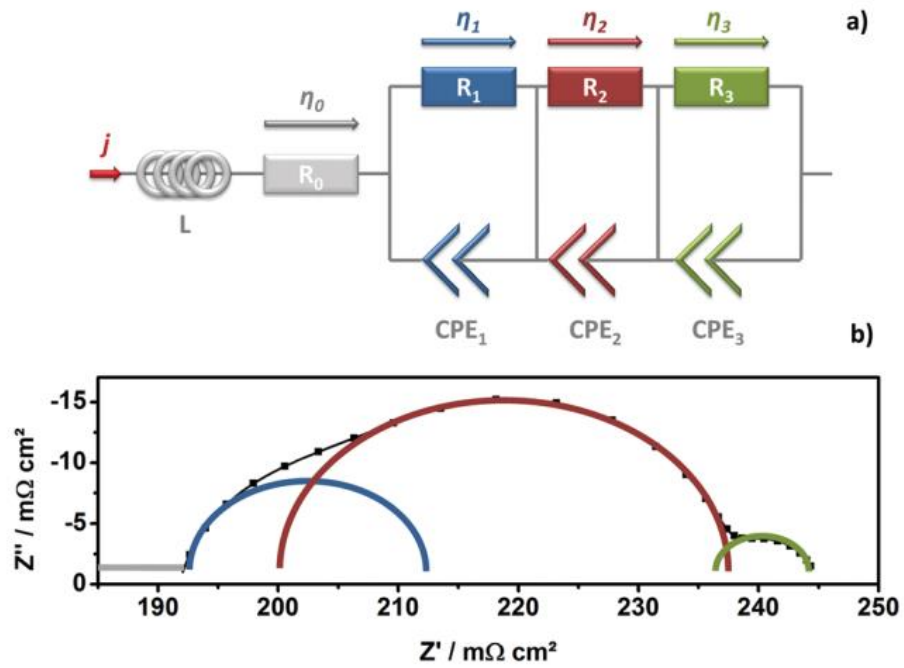
Figure 15 – (a) Equivalent circuit for analysis of the Nyquist diagram in b), (b) example of a Nyquist diagram (extracted from [29]).

3 Materials and Methods

For this research, electrochemical characterizations of PEM electrolyzer cells with different coated GDL meshes on the anode side were performed. Uncoated meshes were used as reference GDLs. In this phase, it was important to learn how to work with the electrochemical device, test benches and assembly of an electrolyzer. Technical difficulties were detected in the system and measurements, but solutions were quickly found and applied in the following phase. In second phase, an electrochemical characterization of the previous materials was carried out again at least three times to ensure reproducibility and generate error bars. In the third and last phase, one long-term measurement of 500 h was performed for the anode GDL that showed best performance in the previous phase. The work plan for the three phases is presented in **Figure 16**.
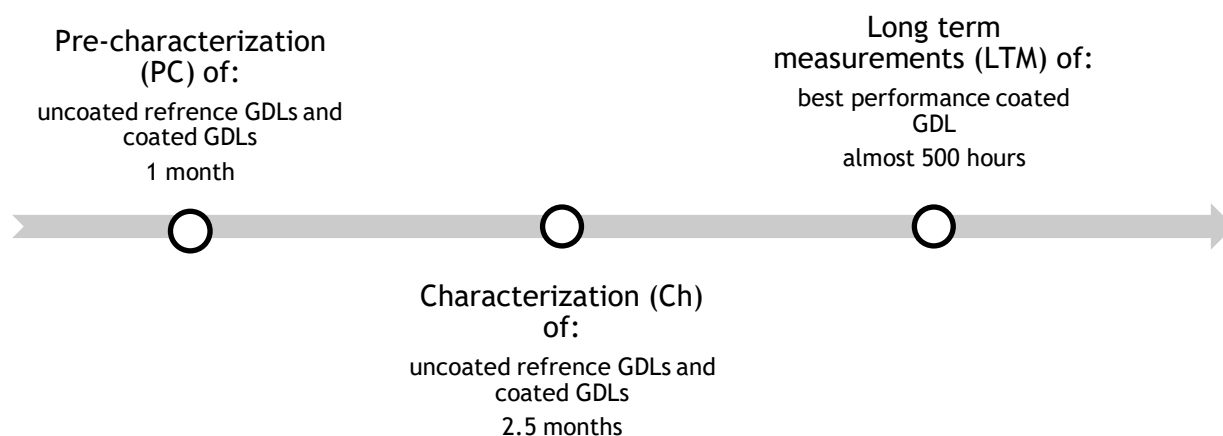

Figure 16 – Work plan of the electrochemical characterization of the GDLs in the PEM electrolyzer cells.

3.1 Materials Used

In this work, the commercial E400 CCM – MEA from Greenerity was used and analyzed. This CCM-MEA is known to be stable with standard loadings and the one of the most used in the market. The GDLs used were made of meshes, sintered powder, cloths or carbon paper. It was tested for the anode side:

- Stainless steel mesh coated with titanium (SS mesh/Ti);
- Stainless steel mesh coated with titanium and niobium (SS mesh/Ti/Nb);
- Titanium mesh coated with titanium (Ti mesh/Ti);
- Titanium mesh coated with titanium and niobium (Ti mesh/Ti/Nb);
- Titanium uncoated mesh;
- Stainless steel uncoated mesh;
- Sintered titanium (sintered Ti) with a titanium net (Ti net).

For the cathode side it was used stainless steel mesh (SS thin mesh) with carbon paper. The different thicknesses of these GDLs are summarized in **Table 2.**

All the meshes with a MPL of niobium and/or titanium were created by VPS in DLR, with the enthalpy parameters in **Table 2**. They were pre-heated at 250 ℃ before deposition and had a torch sweep rate of 350 mm·s^{-1} inside a chamber pressure of 50 mbar. This chamber pressure was to prevent the presence of oxygen that would oxidize titanium into titanium dioxide. To get the highest enthalpy possible, the flow rates of Ar, N_2, and H_2 were chosen accordingly.

Table 2 – Enthalpy parameters of the vacuum plasma spraying coatings for the coated GDLs as well as the thickness of all GDLs.

GDL	Enthalpy for the VPS coating/ MJ·kg^{-1}	Thickness/ μm
SS mesh/Ti	12.5	4120
SS mesh/Ti/Nb	12.5/21.3	4010
Ti mesh/Ti	12.5	3520
Ti mesh/Ti/Nb	12.5/21.3	3460
Ti uncoated mesh	-	3240
SS uncoated mesh	-	4270
Sintered Ti + Ti net	-	1190 + 710
SS thin mesh	-	1760
Carbon paper	-	280

For the substrates and uncoated meshes it was used stainless steel 316L and titanium grade 1 from TLS Technik Spezialpulver. The stainless steel 316L meshes were 98.5 % cheaper than the titanium grade 1 [52], [53]. The titanium and niobium powder prices for the VPS coatings were similar to each other for a weight of 100 g [54], therefore the coated stainless steel meshes were cheaper than the titanium ones.

SEM images were taken before the experiments to analyze the thickness of the MPL in the coated and uncoated meshes and also to evaluate how the particles of the coatings were distributed on the substrate. These measurements took place in the FE-SEM Zeiss ultra plus (field emission SEM). The working distance had values between 7.9 and 8.2 mm, and the accelerating potential was 20 kV. The detector was the angle selective backscattered (AsB) since it is the detector most suitable to see material differences due to color contrast.

The carbon paper was the TGP-H-090 from Toray.

BPPs without flow field were used in all measurements of the experiments. It was used BPPs made of stainless steel coated with titanium on the anode side to avoid corrosion, while for the cathode side was used stainless steel.

3.2 PEM Electrolyzer Assembly and Test Bench

The test bench was operating with one assembly at a time of a PEM electrolyzer cell. All cell configurations were submerged in a DI water bath with > 0.1 µS·cm^{-1} of conductivity, at 65 ºC controlled by a heating plate, with Teflon balls in the surface to reduce the evaporation and with pins making the connection between the BPP and a power supply. An ion-exchange resin (630 Laurent, GRANBY, QC, J2G 8V1, Aldex Chemical Co LTD) was placed to possible trap the unwanted metallic ions from the stainless steel and the ions resulting from the degradation of the MEA. An agitation stirrer was also present to maintain the water temperature constant.

For the assembly of the sintered titanium GDL, the cell configuration is the one in **Figure 17,** where number is 3 corresponds to sintered titanium. For the other measurements of the coated GDL, the number 2 (titanium net) does not exist.

1 – BPP of the anode side
2 – Titanium net
3 – GDL of the anode side
4 – MEA
5 – Carbon paper (GDL cathode side)
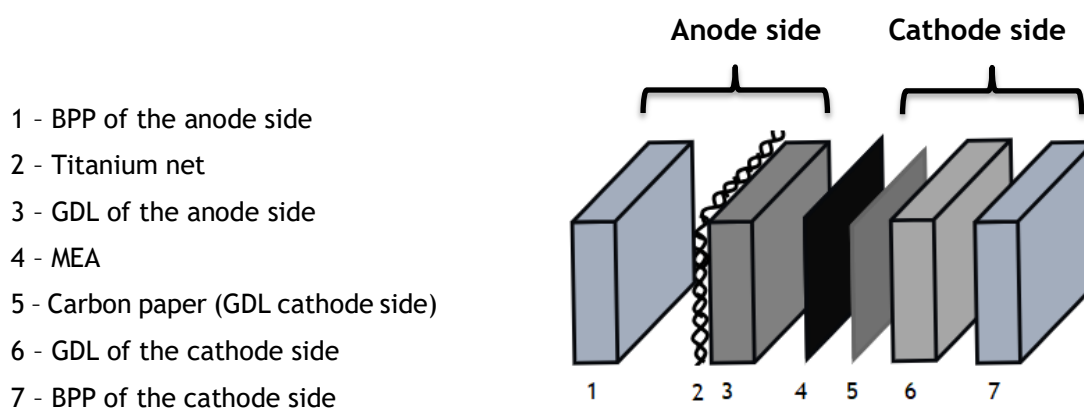6 – GDL of the cathode side
7 – BPP of the cathode side

Figure 17 – Schematic representation of the cell configuration used in the PEM electrolyzer cells with an active area of 4 cm^2.

The active area for the GDLs and MEA was 4 cm^2, even though the MEA itself had a larger area to prevent to be in contact with the GDL and producing a short circuit. **Table 3** shows the different types of cell configurations that were used in this research, where the numbers are associated to **Figure 17,** while being also related to the work plan phase of **Figure 16.**

Table 3 – Different cell configurations used in the experiments and their respective workplan phase.

Work plan	Number in the cell configuration of Figure 17						
	1	2	3	4	5	6	7
P, Ch	Stainless steel coated with titanium	-	SS mesh/Ti	E400	Carbon paper	SS thin mesh	Stainless steel
			SS mesh/Ti/Nb				
			Ti mesh/Ti				
			Ti mesh/Ti/Nb				
		Ti net	Sintered Ti				
Ch			Ti uncoated mesh				
		-	SS uncoated mesh				
LTM			Best coated GDL				

The GDLs made of titanium were cleaned with sulfuric acid, while the ones made of stainless steel were cleaned with DI water. Later, they were inserted in an ultrasonic bath and then were heated in the oven for drying. To close the cell, a torque key was used to cross tightening the screws and to guarantee more mechanical stability.

3.3 Pre-Characterization and Characterization Measurements

For every cell configuration of the pre-characterization phase, three assemblies were done and for each of them it was performed an electrochemical characterization of one polarization curve and one EIS experiments. The polarization curve was obtained till 2 A·cm^{-2}, according to the manual from Joint Research Centre and Fuel Cells and Hydrogen Joint Undertaking [55]. The EIS was performed with an impedance module (Zahner PP240), in galvanostatic mode from 100 mHz to 50 kHz of frequency and amplitudes between 50 mA and 200 mA. The input current was 400 mA, 1 A, 2 A, 4 A and 8 A.

Later, for the characterization step it was performed three polarization curves till 2 A·cm^{-2} and back with a scanning rate of 16 mA·s^{-1}. Additionally, a polarization curve as well with EIS analysis were obtained three times for the same assembly (three trials) with the same parameters as mentioned before; the cell was then reassembled and a new cycle of three reads obtained. This procedure originated a set of 9 polarization curves and EIS spectra for the same cell configuration and operating conditions.

3.4 Long-Term Measurements

The long-term measurements had the goal to observe degradation of the system in an accelerated stress test (AST) conditions at 65 ℃, with a constant input of high current/potential for 500 h.

With this in mind, for the long-term measurement of the chosen best performance coated GDL it was performed an electrochemical characterization of two polarization curves followed by the EIS experiments, with the same parameters mentioned before. Afterwards, the AST test was done at constant current density and the values for the potential over time were registered. In terms of safety, the installation was prepared to stop the experiment if the cell potential would reach 2.4 V. It was added DI water twice a day to the cell, since it was consumed in the reaction rapidly. The installation system was not able to operate on the weekends, so it was necessary to shut it down by the end of every week. An electrochemical characterization of two polarization curves and one EIS experiment were performed every week before the weekend. The ion-exchange resin was also sampled once to observe the ions present in the solution by X-ray photoelectron spectroscopy (XPS) performed in DLR.

After completing the test, dry samples of DI water ion exchange resin were analyzed by X-ray photoelectron spectroscopy (XPS) to quantify the elements trapped in the resin. XPS was done using a Thermo Scientific ECSALAB250 ultra high vacuum facility with a base pressure of $5 \cdot 10^{-10}$ mbar. It was used a standard Al Kα (Thermo Scientific XR4, 300 W) for the X-ray source. The kinetic electrons were detected using a 6 channeltron hemispherical electron energy with energy resolution of 0.9 eV. The sample was previously vacuum for 5 h, since it was humid from the solution, and then it was pestle. The values of the signal area for each element were calculated by the software and were divided by their atomic subshell photoionization cross sections [56] for 1486.6 eV, giving this way the atomic fraction.

4 Results and Discussion

4.1 Scanning Electron Microscopy (SEM) / Energy Dispersive X-ray Spectroscopy (EDX)

The SEM images of the uncoated and coated GDL meshes are shown in **Figure 18** and **Figure 19**. The black background is the epoxy resin that was used for the sample preparation. The elements with high atomic mass are shown in lighter tones, while the ones with low atomic mass are represented in darker tones. The brightest area corresponds to the Nb layer, since it is the heaviest metal in the samples, while the medium tone areas are stainless steel and titanium. **Figure 18 a)** and **b)** shows the titanium mesh without and with Ti coating, respectively. **Figure 18 c)** and **d)** present the stainless steel mesh, where the first one is coated with Ti while the second one with Ti/Nb. The Ti and Nb coatings have different thicknesses because the number of layers and plasma enthalpies in the coating process were different. **Figure 19 a)** presents another SEM image of the coated titanium GDL mesh with Ti/Nb with a cutaway, shown in **Figure 19 b).**
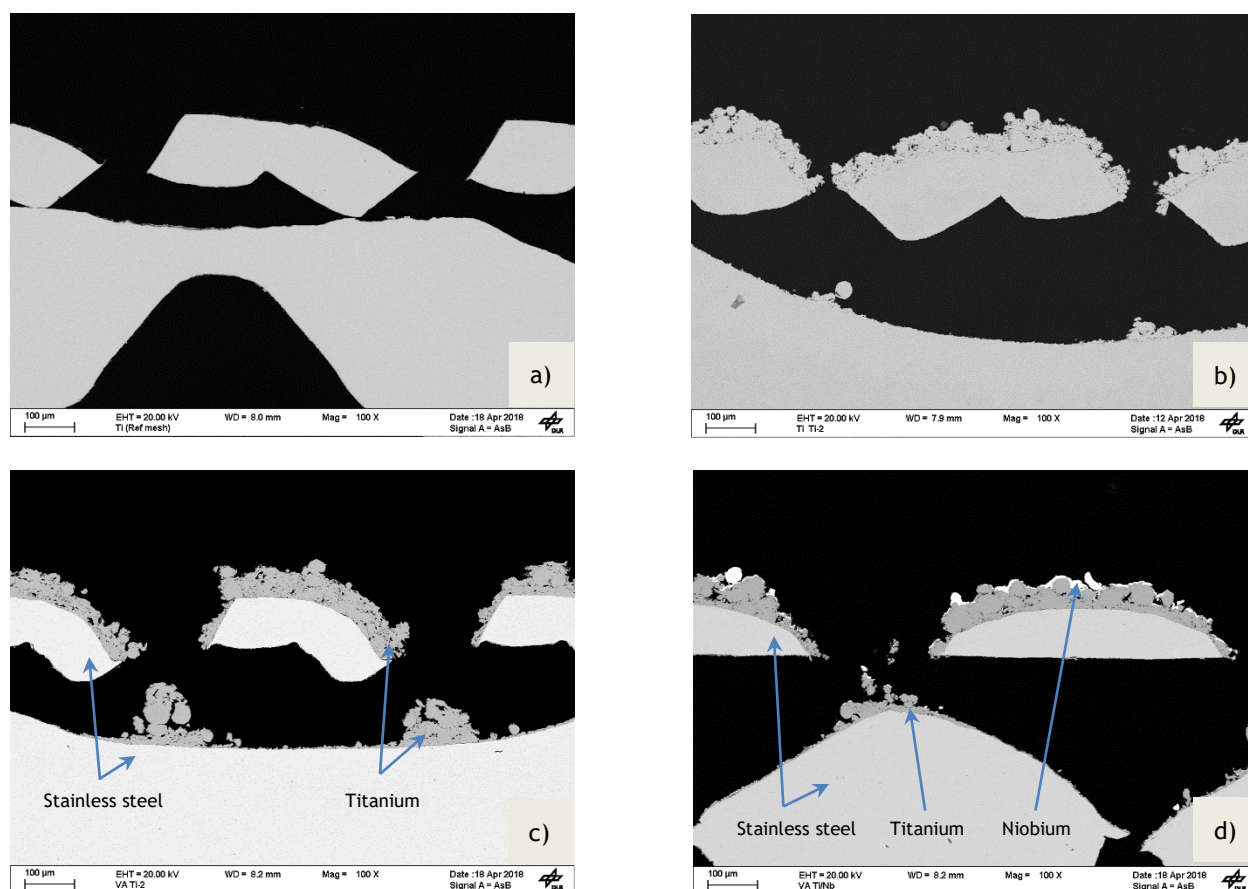

Figure 18 – SEM images of samples from the anode GDLs tested: a) Ti uncoated mesh, b) Ti mesh/Ti, c) SS mesh/Ti, d) SS mesh/Ti/Nb.

One can observe, that the coatings have high rugosity and are well distributed on the substrate, since they cover all GDL surface area. Consequently, the MPL increases the GDL surface area and it should contribute to a higher transportation of electrons, water and the generated oxygen in the anode side.

Interestingly, the plasma sprayed coatings reduce the aperture size of the mesh, which should have an impact in lowering the in-plane resistance of the anode catalyst layer.

The mass fraction of the Ti and Nb coatings was determined by EDX in the selected areas (Mw) of Ti mesh/Ti/Nb of **Figure 19 b)**. The results are summarized in **Table 4**. Oxygen mass fraction is considered to be residual since EDX is not suitable to correctly quantify this light element.
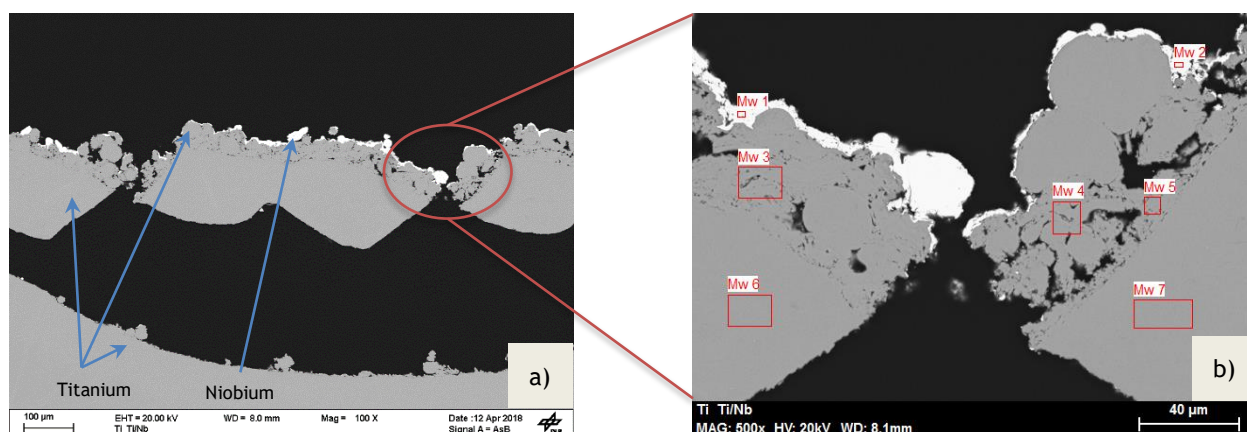

Figure 19 – a) SEM images of sample tested of Ti mesh/Ti/Nb, b) Selected areas for EDX analysis in Ti mesh/Ti/Nb.

As presented in **Table 4**, the mass fraction (mf %) of Nb (Mw 1 and 2) and Ti coating (Mw 3, 4 and 5) on Ti mesh corresponds to *ca.* 97 % and 100 %, respectively. The high purity of the layers is necessary to resist the highly corrosive environment in the anode of the PEM electrolyzer. Areas Mw 6 and 7 are related to Ti substrate.

Table 4 – Mass fraction of the elements in the areas described in **Figure 19 b)** by EDX analysis.

Area designation	Elements/ mf %		
	O	Ti	Nb
Mw 1	2.36	0.91	96.73
Mw 2	2.37	0.79	96.85
Mw 3, 4, 5, 6, 7	-	100.00	-

Figure 20 shows selected areas of SS mesh/Ti/Nb for the EDX analysis represented in **Table 5**. The mass fraction of the elements in the coatings have similar values as the ones in the previous EDX analysis in **Table 4.**

The area Mw 1 and 2 have 96.55 % and 96.12 % of Nb coating, respectively. Area Mw 3 and 4 for shows high purity with 100 % of Ti coating. Important to point out the existence of silicon (Si), chromium (Cr), iron (Fe), nickel (Ni) and molybdenum (Mo) in the areas related to stainless steel substrate, namely Mw 5 and 6. The presence of these elements are in accordance with the composition of the stainless steel 316L used.
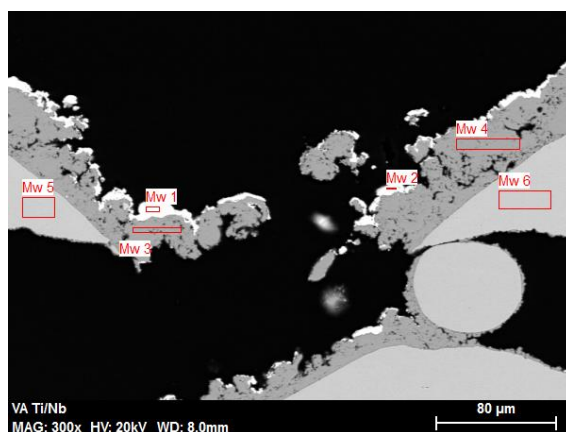

Figure 20 - Selected areas for EDX analysis in SS mesh/Ti/Nb.

Table 5 - Mass fraction of the elements in the areas described in **Figure 20** by EDX analysis.

Designation	Elements/ mf %							
	O	Si	Ti	Cr	Fe	Ni	Nb	Mo
Mw 1	3.12	-	0.35	-	-	-	96.55	-
Mw 2	3.32	-	0.57	-	-	-	96.12	-
Mw 3, 4	-	-	100.00	-	-	-	-	-
Mw 5	0.71	0.39	0.54	16.99	68.93	10.03	-	2.40
Mw 6	0.69	0.31	0.21	17.50	69.57	9.44	-	2.28

EDX images for SS mesh/Ti and Ti mesh/Ti are in **Appendix A** and they also show a high purity in the titanium and niobium coatings.

4.2 Electrochemical Characterization of the Cell Performance

4.2.1 Characterization Measurements

In the characterization measurements it was evaluated the cell performance of coated GDL meshes with niobium and/or titanium and they were compared to the uncoated meshes to investigate the effect on having a macro-porous layer. At first, it was observed that deviations on performance were related to errors on the measurements, stabilization of the impedance device and in the assembly process.

After minimizing errors from the measurements and setup, all the coated and uncoated GDLs were measured several times to ensure reproducibility and generate error bars. For the analysis of the results, it was chosen the assembly and trial that showed more stability and lower slope in the polarization curve for each cell configuration in the different measurements.

Stainless steel is a metal alloy that would preferable be a substitution of state-of-art titanium for the GDL production in the anode side, due to its low cost and easy production method. **Figure 21** represents the cell performance of uncoated stainless steel mesh at 2 A·cm^{-2} where it is clear, on both trials, that this cell configuration does not show a stable curve. The trials were performed on a five minutes time difference. The slope is too high and the curve itself is not linear, reaching 2.4 V at 0.73 A·cm^{-2} in the first trial. These results show a clear pathway of corrosion, that might be related to the formation of an oxide layer in the stainless steel surface attributed to both oxidation reaction and diffusion mechanisms [57]. Mo *et al*. (2015) identified corrosion elements of iron and nickel that were transported from the anode to the cathode and across the CCM through electrochemical migration [57]. **Figure 21** is in accordance with Mo *et al*. since it shows an exponential increase related to ohmic resistance, or, in other words, due to a high resistance in an efficient transport of the electrons and formed product gases in the GDL.
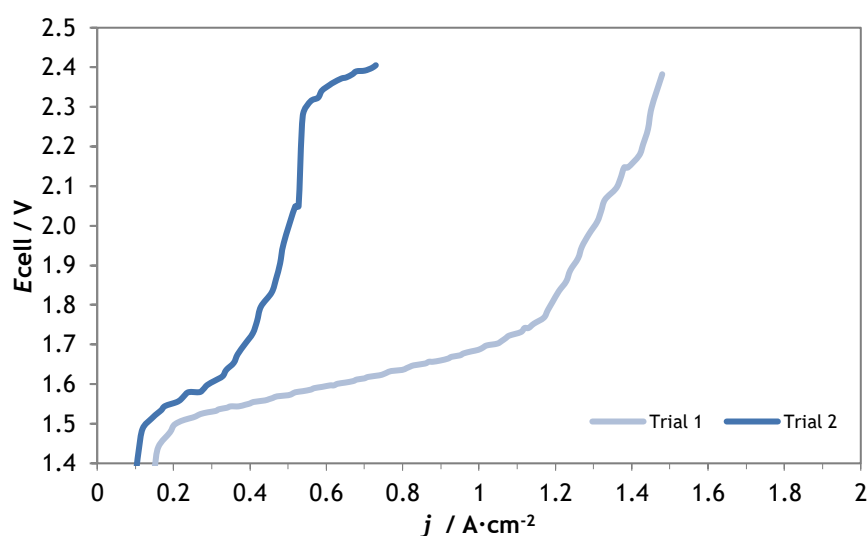

Figure 21 - Polarization curve of uncoated SS mesh at 2 A·cm^{-2}, 65 ºC, atmospheric pressure and with an active area in the cell components of 4 cm^2. Trial #1 and #2 have a five minute difference.

In short, stainless steel meshes cannot be used as anode GDLs in PEM electrolyzers unless these meshes are well protected against corrosion.

The polarization curves of the cells with the coated GDLs are represented in **Figure 22**. The characteristic with the uncoated Ti GDL mesh and sintered titanium are also included in the figure for comparison purposes. At current densities below 0.4 A·cm^{-2}, the curves almost overlap each other, but at higher current densities the uncoated Ti mesh shows already a rapid increase in potential. Therefore, this shows that the uncoated Ti mesh has higher ohmic resistance when compared to the other tested GDLs, since it reveals the highest slope. Additionally, the uncoated Ti mesh shows no overlapping between the ascending and descending curve, where this could be related to a high resistance in mass transport [55]. The remaining GDLs have a linear increase with values of overpotential below 2 V at 2 A·cm^{-2} at 65°C which is an important known key performance indicator (KPI) for commercial PEM electrolyzers [17].

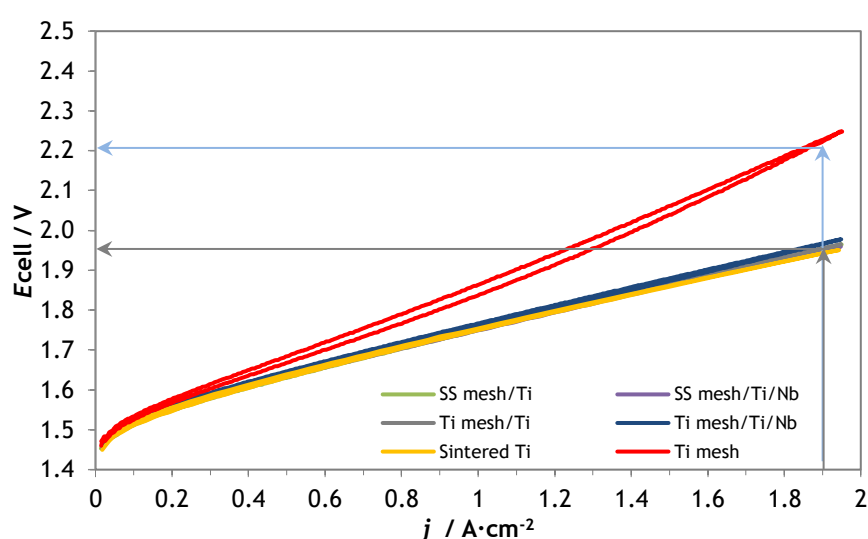Figure 22 - Polarization curve of the coated and uncoated meshes at 2 A·cm^{-2} at 65 ºC, atmospheric pressure and with an active area in the cell components of 4 cm^2.

Figure 23 shows the values of overpotential for the different cell configurations mentioned in **Figure 22**, at 2 A·cm^{-2}. Their respective error bars are associated to different assemblies. The coated Ti mesh showed a remarkable improvement in performance of 324 mV when compared to the uncoated mesh. To point out that sintered titanium also showed similar performances with the coated meshes. The stainless steel meshes showed the most stable results, since their error bars do not differ as much as in the other GDLs.
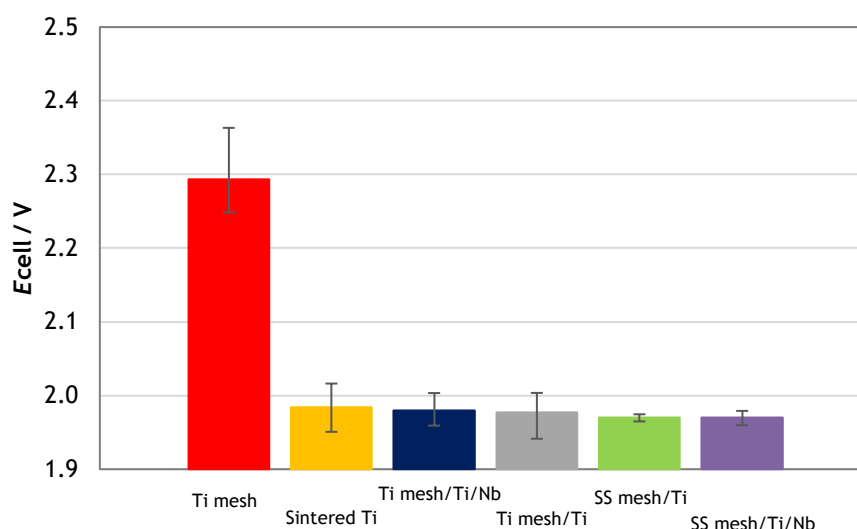
Figure 23 – Values of overpotential reached at 2 A·cm⁻² for the different cell configurations at 65 °C.

The polarization curves can also give information concerning the PEM electrolyzer cell efficiency. The efficiency of a PEM electrolyzer is related to the cell potential where the lowest potential values mean a higher efficiency. On the other hand, the current density is related to amount of hydrogen produced. For the purpose of knowing the efficiency of the PEM electrolyzer cells, it was assumed that the supplied current was converted completely into the electrochemical reaction of electrolysis. Therefore, and according to **Equation (5)** and (**6**), the cell potential would be 1.48 V for a 100 % efficiency if all the input energy was electrical. In **Equation (12)**, $\varepsilon_v^{\mathrm{HHV}}$ represents the efficiency for the high heating value (HHV) of hydrogen, while $E(T)$ represents the potential at given temperature and E^0 represents 1.48 V.

$$\varepsilon_v^{\mathrm{HHV}} = \frac{E^0}{E(T)} \tag{12}$$

Table 6 compares the efficiency values between the uncoated Ti mesh and the remaining tested GDLs for the current density of 1.9 A·cm⁻². As can be seen, coating a MPL in the anode GDL is helping accomplishing the target for 2030 on having more than 80 % [17] efficiency in a PEM electrolyzer. The sintered titanium GDL is moving also towards the KPI for efficiency by 2030, however, the production costs are too high when compared to other GDLs such as meshes.

Table 6 – Efficiency of uncoated Ti mesh in comparison to the coated meshes and sintered titanium for 1.9 A·cm⁻² of current density and input power need in the system.

	Potential measured/ V	$\varepsilon_v^{\mathrm{HHV}}$/ %	KPI of efficiency for 2030/ %	Power/ W
Ti uncoated mesh	2.23	66.4		16.9
Coated GDLs and sintered titanium	1.95	75.9	> 80 [8]	14.8

All things considered, decreasing the overall potential with the use of a MPL helps decreasing the power input in the PEM electrolyzer system, since power is the multiplication of potential and current. Consequently, the operation costs would decrease, as well as the number of cells needed in a stack. It is important to realize that the coated SS meshes exhibit a considerably increase in performance and range of operation when compared to the uncoated SS mesh in **Figure 21.** The MPL improves the contact between the components in the PEM electrolyzer, while conducting properly the electrons and transporting the formed product gases. The data concerning the effect of a MPL was previously reported by Lettenmeier *et al.* (2016) [16], in which it was demonstrated that Ti coatings on sintered Ti would improve the performance of PEM electrolyzers when operated at high current densities [16]. The data here presented for the stainless steel mesh is in good agreement with this article, showing, once again, that the MPL is the component of a PEM electrolyzer cell where the research and development should focus.

EIS experiments were performed to have a clearer perception on the performance of the cell, but also to obtain more information about the ohmic and mass transport resistances. **Figure 24** and **Figure 25**, show the Nyquist plots of the tested GDLs for 0.25 and 1 A·cm^{-2}, respectively. Uncoated stainless steel mesh was not measured, since it showed bad performance for low current densities in the polarization curve, and therefore its EIS data was not relevant to the study.

Figure 24 shows that the ohmic resistance values for the current density of 0.25 A·cm^{-2} vary between 179 and 206 mΩ·cm^2, and they were calculated from the arc intercept with the real axis in the high frequency region (between 200 kHz and 10 Hz [58]). Data in **Figure 24** shows that the Ti mesh/Ti is the GDL contributing with the smaller ohmic resistance to the PEM electrolyzer cell, while the sintered titanium along with Ti mesh/Ti/Nb have higher resistances values.

The oxygen evolution reaction (OER) at the anode side is the reaction with the largest losses in the cell as well with the slowest kinetics when compared to the hydrogen evolution reaction (HER) in the cathode. The HER is known to be a fast process in acidic aqueous media, and has little contribution for the overall cell impedance [59]. As a result, the arc corresponding to the HER is most likely to not be clearly detected in the EIS measurements, since its activation losses arc were less prominent than the OER [59]. With this in mind, **Figure 24** shows the arc in high frequency range being related to the OER, with summit values of 18.6 Hz for every GDL tested, except for Ti mesh/Ti/Nb that takes the value of 24.7 Hz. These arcs did not present significant deviations, which makes sense since all cell configurations used the same and catalyst loadings in the MEA, therefore presenting similar values for the activation resistance.

However, the high frequency region in **Figure 24** shows, not only the arc associated to OER, but also a second smaller arc in the frequency region higher than 25 Hz. This arc is most visible for Ti mesh/Ti, SS mesh/Ti/Nb and SS mesh/Ti and can be related to the HER, double layer effects in the electrode or charge transfer resistance at the interface between the GDL and the anode catalyst layer [16].

The uncoated titanium mesh is the only GDL showing mass transport losses at 0.25 A·cm⁻², since a second semicircle is already visible for the frequency of 0.1 Hz, related to the low frequency region.
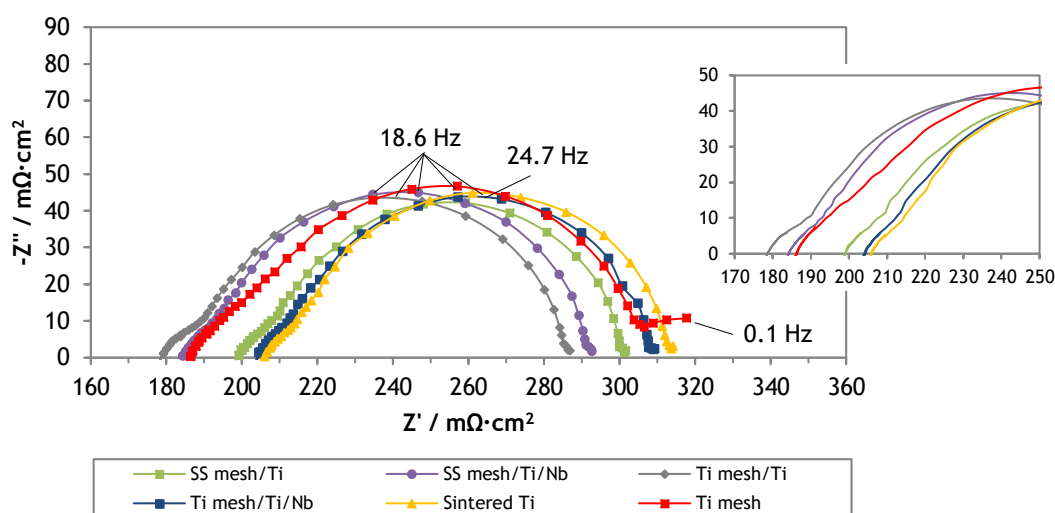
Figure 24 - Nyquist plots from the EIS measurements at 0.25 A·cm^{-2} (amplitude 50 mA). From 100 mHz to 50 kHz of frequency.

With the increase of current density, the uncoated Ti mesh show its EIS characteristics shifting to the right in the X-axis of the graph when compared to its respective measurement at low current density, **Figure 25**. This effect means that the ohmic resistance increases with the current density. A possible cause for this phenomenon could be a high pressure between the electrode and the GDL leading to a partial block of the active areas in the electrode. As a result, the reaction is not taking place with the same rate as before, however, the water is still able to reach the active areas via secondary paths of thin films [29]. Consequently, a gas pillow is formed at the interface that pushes the GLD away from the catalyst layer increasing the ohmic losses [29].

The summit frequency value for the uncoated Ti mesh, in the high frequency region in **Figure 25**, is 134 Hz, while the second arc has 0.100 Hz, showing already that this arc is in the low frequency range. Additionally, is showing a 45º line associated to diffusion and convections mechanisms as mass transport losses [23]. Once again is shown that the uncoated GDL mesh is not diffusing the products as fast as the other tested GDLs.

With these results, is confirmed that the high values of overpotential for the uncoated Ti mesh in the polarization curve are, in fact, due to the existence of mass transport losses. Important to point out that the uncoated Ti mesh also increases its activation losses, since the arc in the high frequency range has higher summit values when compared to the results at low current density. This increase could be related to a possible degradation of the MEA. Analyzing the results for the coated GDLs, practically no increase of ohmic resistance was observed and mass transport effects were negligible.

The results clearly demonstrate the benefits of having a MPL at the interface between the GDL and anode catalyst layer. To have a more detail overview of the electrochemical phenomena, is required a proper simulation and fitting of the curves according to an equivalent electrical circuit. However, this simulation is beyond the scope of this work.
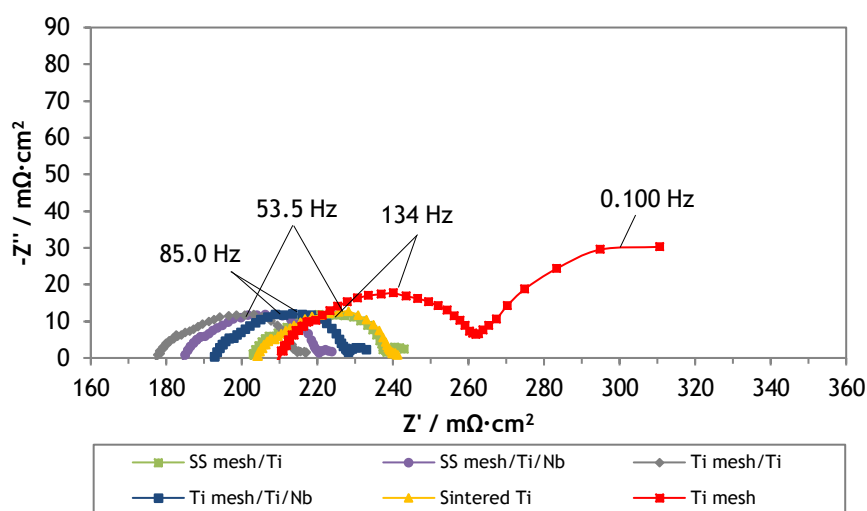

Figure 25 - Nyquist plots from the EIS measurements at 1 A·cm^{-2} (amplitude 200 mA). From 100 mHz to 50 kHz of frequency.

4.2.2 Long-Term Stainless Steel/Ti/Nb Measurements

After electrochemically characterize all cell configurations, it was decided to perform a durability test at constant current density for SS mesh/Ti/Nb, since this cell configuration showed good performances at low and high current densities while being the coated GDL less expensive. This test was carried out at constant current density of 2 A cm^{-2} and operation temperature of 65 ºC. The potential values were recorded over time.

Figure 26 shows the potential evolution of SS mesh/Ti/Nb where the potential values were measured over a period of 435 h. The intermittent potential spikes correspond to the period when it was added cold DI water into the cell, twice a day. When the temperature decreases, the Gibbs free energy also decreases for the same electrical energy input, resulting in a decrease in the reaction kinetics and, therefore, an increase in the overpotential.

In overall, the cell started at 0 h with 1.996 V and shut it down after 435 h with 2.4 V. It is clear the increase of potential over time, meaning that the PEM electrolyzer cell performance was rapidly decreasing. The degradation rate can be related to the amount of potential that increases per unit of time. In this experiment, it was observed 7 degradation rates for a linear behavior of the potential values.
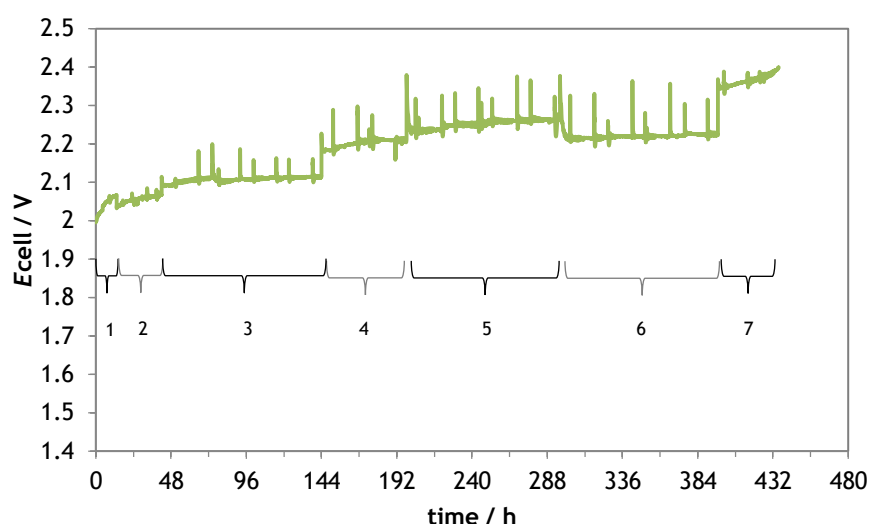

Figure 26 – Long-term testing of SS mesh/Ti/Nb at constant 2 A·cm^{-2} and 65 ºC. The values of potential were recorded over the period of 435 h and it was observed 7 degradation rates.

Table 7 shows the degradation rates related to **Figure 26**. Curve 1 is related to the conditioning of the cell, since it corresponds to the first 24 h, therefore, it is the cell adapting to the operating conditions. Afterwards, the degradation rate decreases in curve 2 and is near zero on curve 3, 4, 5 and 6, meaning that the cell was getting stable over time and potential values did not vary as much as in the beginning. After 144 h the cell shows a significant decrease in efficiency, since the potential values increases. At 296 h the potential values decrease, but quickly becomes stable during the following 100 h. However, at 396 h, the cell performance decreases considerably again reaching 2.4 V, and, consequently, the experiment was shut down.

Table 7 – Degradation rates in the long-term test of SS mesh/Ti/Nb at constant 2 A·cm^{-2}.

Curve number in Figure 26	Time/ h	Degradation rate/ mV·h^{-1}
1	13	4.85
2	42	1.21
3	144	0.02
4	198	0.46
5	292	0.50
6	396	0.04
7	435	1.34

Figure 27 shows the polarization curve evolution during the 435 h. Before beginning the experiment, in time 0 h, the cell shows good performance below 2 V at 2 A·cm^{-2} with a linear behavior. After 56 h, there is evidence of an increase in ohmic resistance since the slope increases. From 144 h on, the curve is showing a decrease in the linear behavior for high current densities, probably due to existence of mass transport losses. Important to realize that, after 296 h the slope of the curve decreases showing an improvement in performance, already mentioned in **Figure 26,** and increases again after 100 h. The polarization curve after 435 h shows a clear exponential behavior related to a high mass transport loss.
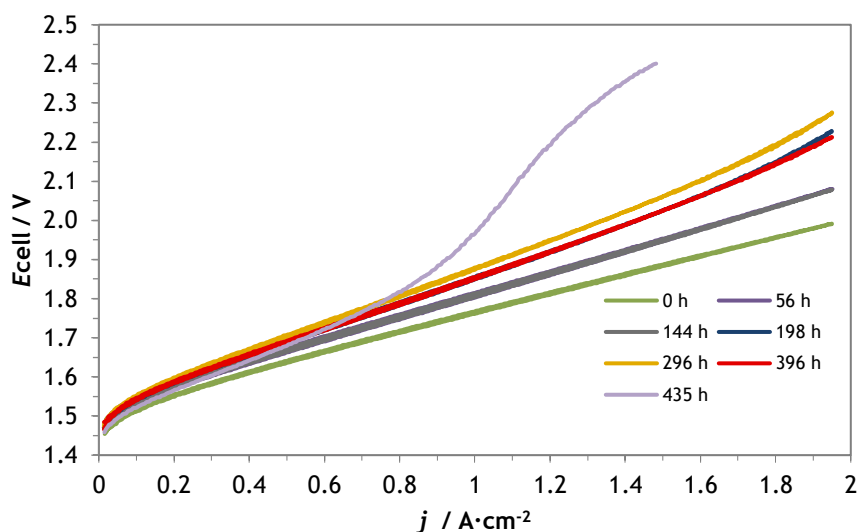

Figure 27 - Polarization curve of long-term measurement of SS mesh/Ti/Nb till 2 A·cm^{-2}, at 65 °C, atmospheric pressure and with an active area in the cell components of 4 cm^2.

The EIS experiments performed at 0.25 A·cm^{-2} and 1 A·cm^{-2} are expressed in **Figure 28** and **Figure 29**, respectively. The Nyquist graph at 0.25 A·cm^{-2}, in **Figure 28,** shows an increasing in ohmic resistance over time. The values start at 187 mΩ·cm^2 and after 435 h the ohmic resistance is 231 mΩ·cm^2. The highest value of ohmic resistance is after 296 h with 244 mΩ·cm^2, which corresponds to the highest slope in the polarization curve.

The activation losses do not have a significant deviation since the summit of the arcs in the high frequency are approximately the same, with values of 18.6 Hz, except for time 0 h that had 24.8 Hz. This can demonstrate that the MEA did not suffer degradation mechanisms at low current densities over time.
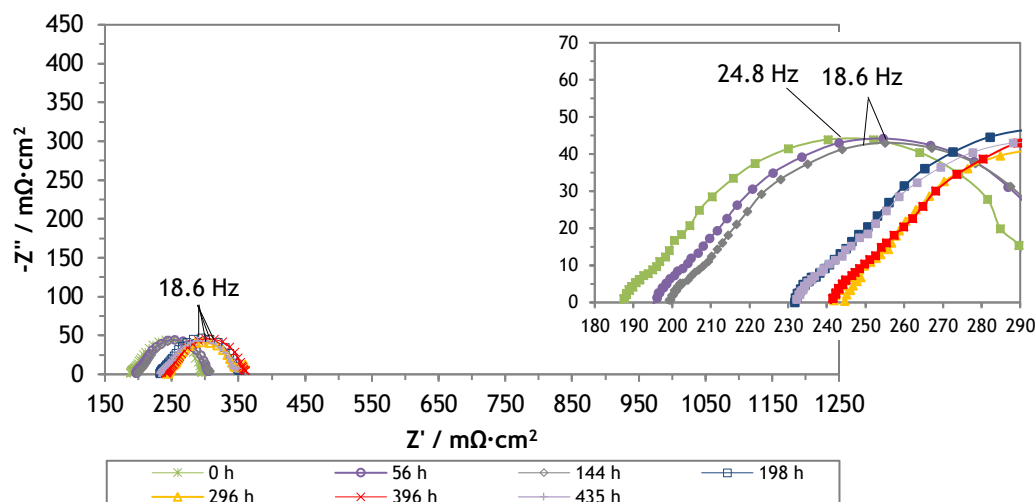

Figure 28 - Nyquist plots from the EIS long-term measurements of SS mesh/Ti/Nb at 0.25 A·cm^{-2} (amplitude 50 mA). From 100 mHz to 50 kHz of frequency.

However, for high current densities shown in **Figure 29,** the values for ohmic resistance increases over time from 188 mΩ·cm^2 to 251 mΩ·cm^2. In the low frequency range, it is now evident arcs related to mass transport, with frequency values of 0.540 Hz for 296 h and 435 h, while the 396 h has 0.312 Hz.
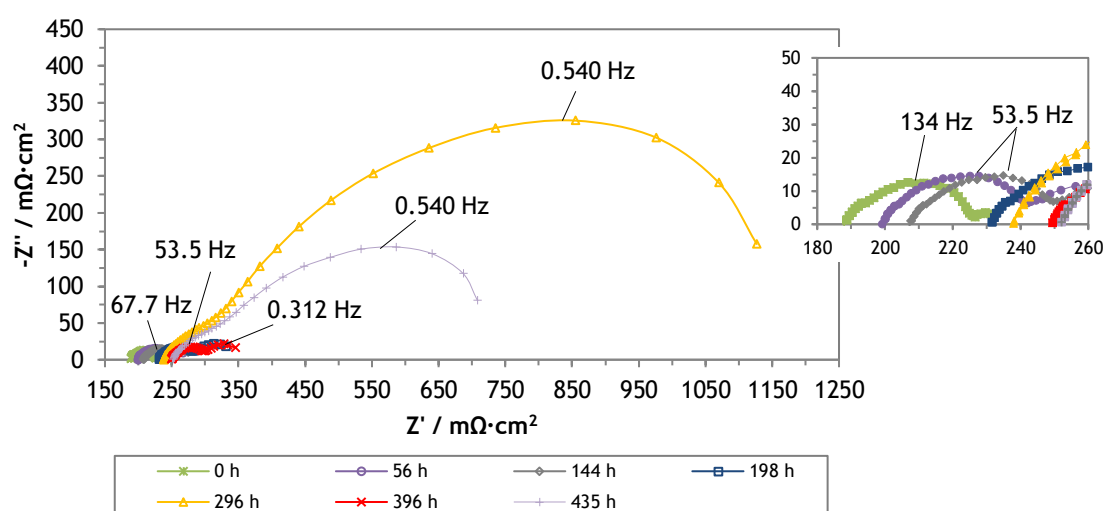

Figure 29 - Nyquist plots from the EIS long-term measurements of SS mesh/Ti/Nb at 1 A·cm^{-2} (amplitude 200 mA). From 100 mHz to 50 kHz of frequency.

Overall, the EIS data is in accordance with the polarization curve and the long-term measurements at constant current density. When the cell potential increases harshly, the polarization curve and EIS show evidence of a degradation mechanism of mass transport. In the same line of thought, if the cell shows an improvement in potential after a certain period of time, then the ohmic resistance values decrease, as well as the slope in the polarization curve. This rapid degradation may be attributed to different factors that occurred during operation, where one of them can be related to the paper bag which contained the DI water ion exchange resin. After 144 h of operation it broke releasing paper particles into the solution. As a result, these particles could move inside the GDL and partially block the pores, therefore increasing the mass transport resistance.

Another plausible reason for the rapid cell degradation is the water contamination by the corrosion products of the stainless steel mesh, in particular iron and chromium ions. Dry samples of DI water ion exchange resin were analyzed by XPS to quantify the elements trapped. The results for the pestle and not pestle samples are presented in **Table 8** in atomic fraction of the detected volume and in **Appendix D**. Carbon, oxygen, and nitrogen are most likely the elements from the resin itself. The sulfur could be both from the PFSA/PTFE membrane and from the resin, but there was no way to know which mass fraction corresponds to them. Neither Fe nor Cr were found, suggesting that the MPL/Ti/Nb protected the stainless steel GDL mesh against corrosion.

Table 8 - XPS measurements in atomic fraction of an ion-exchange resin sample of the long-term test of SS mesh/Ti/Nb at 435 h. The results are for pestle and not pestle samples of resin.

Element	At/ %	
	Pestle	Not pestle
C	63.23	59.31
O	26.67	36.87
N	3.80	1.53
S	6.30	2.27
Si	0.00	0.01

5 Conclusion

Nowadays, studies concerning PEM electrolysis technology have been increasing in the scientific community with the goal to improve its performance and durability while considering the energy market needs. The mission to produce hydrogen through a viable economical pathway is getting more tangible each day. Especially, with the attractive outlook of having a zero-cost main source of electricity when this one is derivate from the intermittence of renewable sources. Several efforts have been made to tackle some difficulties that are still associated to this technology, such as CAPEX costs related to stack components manufacturing.

As mentioned in the introduction chapter, the state of art of this work had its focus on giving a summary on the developments reported so far to decrease the production costs of a PEM electrolyzer stack. Researches on low cost catalysts and different loadings on the MEA are one of the options to consider to PEM electrolysis become more cost-effective, however, improvements on the manufacturing and coatings of gas diffusion layers and bipolar plates are most likely to decrease substantially the stack cost. In the first place, it was reported that removing the flow field from the manufacturing of bipolar plates and insert it into the gas diffusion layer would decrease the overall costs. Secondly, it was also proved that low cost metals with coatings by vacuum plasma spraying for the production of bipolar plates had remarkable performances. This last concept was also applied for the manufacturing of low cost gas diffusion layers on the anode side, with coatings of macro-porous layers.

Following this assumption, the work here presented shows results of performance and durability of low cost gas diffusion layers meshes coated with porous layers of Ti and Nb for the anode side and with a flow field integrated.

For the morphology characterization of the samples it was performed scanning electron microscopy to analyze the thickness of the coatings and to concluded that the particles were well distributed on the substrate. The elemental composition, through energy dispersive X-ray detector, showed a porous layer with high purity of Ti and Nb.

The PEM electrolyzer cell components had a 4 cm^2 active area and were properly cleaned and assembled before each set of experimental tests. The different cell configurations were submerged in a deionized water bath, at 65 ºC, with an ion-exchange resin to possible trap the unwanted metallic ions. Several trials and assemblies were performed to ensure reproducibility and to generate error bars.

Electrochemical characterization was performed through polarization curves and EIS experiments in impedance devices to evaluate, not only the performance of the different cell configurations, but also the major contributions for the decrease of the real potential in the cell.

The polarization curve of the stainless steel mesh coated with Ti and Nb showed a reduction in overpotential of 324 mV at 2 A·cm^{-2} when compared to the uncoated titanium mesh used currently in large industry PEM electrolyzers stacks. This result means an improvement on efficiency of ca. 10 %, therefore suggesting that Ti/Nb coatings were able to protect the gas diffusion layer against corrosion at the same time as they assign high catalytic activity characteristics.

Additionally, all coated gas diffusion layers meshes showed an almost complete elimination of mass transport losses at low and high current densities when compared to the uncoated ones, as it was confirmed from the Nyquist plots.

A long-term experiment of 435 h was performed for the stainless steel mesh coated with Ti and Nb, where it showed a rapidly increase of potential over time, mainly due to technical difficulties found in the electrolyzer setup. Actually, the observed degradation was assigned to mass transport losses, where no activation overpotential increase was observed. Moreover, the analysis of the ion-exchange resin showed no traces of metallic ions or other corrosion products from the stainless steel, suggesting that the gas diffusing layer suffered no corrosion.

All things considered, the vacuum plasma spraying technology was successfully used for coating the macro-porous layer in the low cost gas diffusion layer. This macro-porous layer was capable to prevent the corrosion in the acid medium of the anode side, and therefore improving the durability of a PEM electrolyzer cell. This approach can potentially reduce the capital cost of PEM electrolyzers for large-scale hydrogen production from renewable sources.

6 Assessment of the Work Done

6.1 Objectives Achieved

The scope of this work was to investigate the performance and durability of low-cost coated gas diffusion layers in a 4 cm^2 PEM electrolyzer cell. The performance assessment was analyzed by electrochemical characterization, in particular, through the study of Nyquist diagrams and polarization curves. Several trials and assemblies were performed to ensure reproducibility and to generate error bars. The durability of the GDLs was assessed through a long-term measurement test of 435 h at constant current density. In the long-term experiment, although the cell potential rapidly increased over time, it was still possible to characterize electrochemically the PEM electrolyzer and analyze the degradation mechanisms.

6.2 Other Work Carried Out

Along with the reported research, additional work was carried out. It was performed long-term measurements of a PEM electrolyzer cell with 4 cm^2 of active area with a constant potential of 2 V where the values of current were registered over time at 65 ℃. The cell had a setup similar to the long-term test of SS mesh/Ti/Nb, however, without an agitation steer nor an ion-exchange resin. Sintered titanium with a titanium net was used for the anode GDL and platinum cloth along with carbon paper was used for the cathode GDL. For these measurements, it was tested different MEAs: 400 h with MEA E400, 85 h with a MEA produced in DLR and more than 500 h with MEA E500. It was also performed two polarization curves and one EIS experiment in two moments: before the beginning of the test and before shutting it down, with the same parameters mentioned in the long-term test of SS mesh/Ti/Nb.

Appendix E shows the long-term measurements and polarization curve for MEA E500, since it was the one with less technical problems in the measurements. Additionally, every week was sampled 10 mL of DI water for future analysis by inductively coupled plasma mass spectrometry (ICP-MS). This analysis is outside the scope of this work.

6.3 Limitations and Future Work

Overall, for a better understanding of the results more time was needed to make extra electrochemical analysis. For instance, the electrochemical results that were presented here could be converted to an equivalent circuit and through this study would be possible to have data concerning the electrochemical reactions. Additionally, some technical difficulties in the electrolyzer setup were an obstacle to achieve 1000 h for the long-term measurements. Particularly, the limitation of refilling cold DI water to the system had the negative outcome of punctually worsening the cell performance, since the overpotential increased with the decrease of temperature. For future work, as well as tackling the technical difficulties in a 4 cm^2 PEM electrolyzer, it would be interesting to take the step to a 25 cm^2 PEM cell and characterize the performance and durability of the coated stainless steel GDL meshes.

6.4 Final Assessment

Developing this research project abroad had numerous positive impacts to me, my growth and development, knowledge and career. It was very rewarding to feel that this work is going to open new doors in the scientific community and that contributed to the grow of DLR in the topic of PEM electrolyzers.

This project also gave me an important insight and know-how in topics that I was not comfortable before, such as electrochemistry. I developed my soft skills since I worked in a distinguished multicultural company with experience people that shared their knowledge with me.

References

[1]   S. Abrar, P. De Bonis, D. Buttle, G. Filippo, J. J. Mingo, K. Firkaviciuté, N. Quental, and J. Schuppers, "Strategic Energy Technology (SET) Plan," European Union, Luxembourg, 2007.

[2]   European comission, "EU energy in figures," Luxembourg, 2017.

[3]   "Resolução do Conselho de Ministros n.º 29/2010 of 15 of april of 2010," in *Diário da República, 1ª série - Nº 73*, 2010, p. 1294.

[4]   REN, "Dados técnicos - Technical Data 2015," REN, Lisbon, 2015.

[5]   A. Sternberg and A. Bardow, "Power-to-What? – Environmental assessment of energy storage systems," *Energy Environ. Sci.*, vol. 8, no. 2, pp. 389–400, 2015.

[6]   US Department of Energy, "Hydrogen Production." Fuel Cell Technologies office, United States, 2014.

[7]   D. Fraile, J.-C. Lanoix, P. Maio, A. Rangel, and A. Torres, "Overview of the market segmentation for hydrogen across potential customer groups based on key application areas," 2015.

[8]   International Energy Agency, "Technology Roadmap - Hydrogen and Fuel Cells," France, 2015.

[9]   B. Coelho, A. C. Oliveira, and A. Mendes, "Concentrated solar power for renewable electricity and hydrogen production from water - A review," *Energy Environ. Sci.*, vol. 3, no. 10, p. 1403, 2010.

[10]   G. Maag, G. Zanganeh, and A. Steinfeld, "Solar thermal cracking of methane in a particle-flow reactor for the co-production of hydrogen and carbon," *Int. J. Hydrogen Energy*, vol. 34, no. 18, pp. 7676–7685, 2009.

[11]   N. Assanee and C. Boonwan, "State of the art of biomass gasification power plants in Thailand," *Energy Procedia*, vol. 9, pp. 299–305, 2011.

[12]   A. Houaijia, S. Breuer, D. Thomey, C. Brosig, J. P. Säck, M. Roeb, and C. Sattler, "Solar hydrogen by high-temperature electrolysis: Flowsheeting and experimental analysis of a tube-type receiver concept for superheated steam production," *Energy Procedia*, vol. 49, pp. 1960–1969, 2013.

[13]   T. Smolinka, E. Ojong, and T. Lickert, "Fundamentals of PEM Water Electrolysis," in *PEM Electrolysis for Hydrogen Production: Principles and Applications*, D. Bessarabov, H. Wang, H. Li, and N. Zhao, Eds. Taylor & Francis Group, 2016, pp. 11–32.

[14]   Ö. F. Selamet, F. Becerikli, M. D. Mat, and Y. Kaplan, "Development and testing of a highly efficient proton exchange membrane (PEM) electrolyzer stack," *Int. J. Hydrogen Energy*, pp. 11481, 11482, 2011.

[15]   T. Riis, E. Hagen, P. Vie, and Ø. Ulleberg, "Hydrogen Production and Storage: R&D Priorities and Gaps," France, 2006.

[16]   P. Lettenmeier, R. Wang, R. Abouatallah, S. Helmly, T. Morawietz, R. Hiesgen, S. Kolb, F. Burggraf, J. Kallo, A. S. Gago, and K. A. Friedrich, "Durable Membrane Electrode Assemblies for Proton Exchange Membrane Electrolyzer Systems Operating at High Current Densities," *Electrochim. Acta,* pp. 502–511, 2016.

[17]   L. Bertuccioli, A. Chan, D. Hart, F. Lehner, B. Madden, and E. Standen, *Study on development of water electrolysis in the EU*. Fuel Cells and Hydrogen Joint Undertaking, 2014.

[18]   K. A. Friedrich, "Studie über die Planung einer Demonstrationsanlage zur Wasserstoff - Kraftstoffgewinnung durch Elektrolyse mit Zwischenspeicherung in Salzkavernen," 2015.

[19]   N. Din, A. Ranjbari, L. Catala, F. Brisset, P. Millet, and A. Aukauloo, "Implementing molecular catalysts for hydrogen production in proton exchange membrane water electrolysers," *Coord. Chem. Rev.*, vol. 256, no. 21–22, 2012.

[20]   S. A. Grigoriev, P. Millet, S. A. Volobuev, and V. N. Fateev, "Optimization of porous current collectors for PEM water electrolysers," *Int. J. Hydrogen Energy*, vol. 34, no. 11, pp. 4968–4973, 2009.

[21]   L. Mingyi, Y. Bo, X. Jingming, and C. Jing, "Thermodynamic analysis of the efficiency of high-temperature steam electrolysis system for hydrogen production," *J. Power Sources*, 2008.

[22]   R. O' Hayre, S.-W. Cha, W. Colella, and F. Prinz, *Fuel Cell Fundamentals*, Third. United States of America: John Wiley & Sons, 2016.

[23]   X. Z. Yuan, C. Song, H. Wang, and Z. J., *Electrochemical Impedance Spectroscopy in PEM Fuel Cells: Fundamentals and Applications*. 2010.

[24]   Siyavula, "Activation Energy And The Activated Complex." [Online]. Available: https://www.siyavula.com/read/science/grade-11/energy-and-chemical-change/12-energy-and-chemical-change-03. [Accessed: 01-Jul-2018].

[25]   N. Briguglio and V. Antonucci, "Overview of PEM Electrolysis for Hydrogen Production," in *PEM Electrolysis for Hydrogen Production: Principles and Applications*, D. Bessarabov, H. Wang, H. Li, and N. Zhao, Eds. Taylor & Francis Group, 2016, pp. 1–10.

[26]   M. Carmo, W. Luke, and D. Stolten, "Electrocatalysts for the Hydrogen Evolution Reaction," in *PEM Electrolysis for Hydrogen Production: Principles and Applications*, D. Bessarabov, H. Wang, H. Li, and N. Zhao, Eds. Taylor & Francis Group, 2016, pp. 65–86.

[27]   A. Marshall, B. Borresen, G. Hagen, and M. Tsypkin, "Hydrogen production by advanced proton exchange membrane (PEM) water electrolysers—Reduced energy consumption by improved electrocatalysis," *Energy*, vol. 32, no. 4, pp. 431–436, 2007.

[28]   P. Lettenmeier, R. Wang, R. Abouatallah, F. Burggraf, A. S. Gago, and K. A. Friedrich, "Coated Stainless Steel Bipolar Plates for Proton Exchange Membrane Electrolyzers," *J. Electrochem. Soc.*, vol. 163, no. 11, pp. F3119-F3124, 2016.

[29]   P. Lettenmeier, S. Kolb, N. Sata, A. Fallisch, L. Zielke, S. Thiele, A. S. Gago, and K. A. Friedrich, "Comprehensive investigation of novel pore-graded gas diffusion layers for high-performance and cost-effective proton exchange membrane electrolyzers," *Energy Environ. Sci.*, vol. 10, no. 12, pp. 2483–2654, 2017.

[30] P. Lettenmeier, A. S. Gago, and A. K. Friedrich, "Protective Coatings for Low-Cost Bipolar Plates and Current Collectors of Proton Exchange Membrane Electrolyzers for Large Scale Energy Storage from Renewables," *New Technol. Prot. Coatings*, pp. 69–86, 2017.

[31] Y. Tanaka, K. Kikuchi, Y. Saihara, and Z. Ogumi, "Investigation of current feeders for SPE cell," *Electrochim. Acta*, vol. 50, no. 22, pp. 4344–4349, 2005.

[32] FuelCellStore, "Titanium Screen Mesh Cloth." [Online]. Available: http://www.fuelcellstore.com/titanium-screen-mesh-cloth. [Accessed: 17-Jun-2018].

[33] Y. Zhang, M. D. Merrill, and B. E. Logan, "The use and optimization of stainless steel mesh cathodes in microbial electrolysis cells," *Int. J. Hydrogen Energy*, vol. 35, no. 21, pp. 12020–12028, 2010.

[34] C. M. Hwang, M. Ishida, H. Ito, T. Maeda, A. Nakano, Y. Hasegawa, N. Yokoi, A. Kato, and T. Yoshida, "Influence of properties of gas diffusion layers on the performance of polymer electrolyte-based unitized reversible fuel cells," *Int. J. Hydrogen Energy*, vol. 36, no. 2, pp. 1740–1753, 2011.

[35] H. Ito, "Current Collectors (GDLs) and Materials," in *PEM Electrolysis for Hydrogen Production: Principles and Applications*, D. Bessarabov, H. Wang, H. Li, and N. Zhao, Eds. Taylor & Francis Group, 2016, pp. 147–156.

[36] H. Ito, T. Maeda, A. Nakano, C. M. Hwang, M. Ishida, A. Kato, and T. Yoshida, "Experimental study on porous current collectors of PEM electrolyzers," *Int. J. Hydrogen Energy*, vol. 37, no. 9, pp. 7418–7428, 2012.

[37] H. Ito, T. Maeda, A. Nakano, A. Kato, and T. Yoshida, "Influence of pore structural properties of current collectors on the performance of proton exchange membrane electrolyzer," *Electrochim. Acta*, vol. 100, pp. 242–248, 2013.

[38] P. Lettenmeier, S. Kolb, F. Burggraf, A. S. Gago, and K. A. Friedrich, "Towards developing a backing layer for proton exchange membrane electrolyzers," *J. Power Sources*, vol. 311, pp. 153–158, 2016.

[39] Oerlikon Metco, "An Introduction to Thermal Spray," no. 6, pp. 8–11, 2016.

[40] F. Azarmi, "Vacuum plasma spraying," Toronto, 2005.

[41] W. Zhou, Z. Wang, and D. Joy, *Scanning Microscopy for Nanotechnology: Techniques and applications*. New Orleans: Springer, 2006.

[42] V. Channam, "Synthesis of strongly correlated oxides and investigation of their electrical and optical properties," Institut National Polytechnique de Toulouse, 2017.

[43] S. Swapp, "Scanning Electron Microscopy (SEM)." [Online]. Available: http://serc.carleton.edu/research_education/geochemsheets/techniques/SEM.html. [Accessed: 08-Jun-2018].

[44] C. Wang, "Bipolar Plates and Plate Materials," in *PEM Electrolysis for Hydrogen Production: Principles and Applications*, D. Bessarabov, H. Wang, H. Li, and N. Zhao, Eds. Taylor & Francis Group, 2016, pp. 135–146.

[45] P. Lettenmeier, R. Wang, R. Abouatallah, B. Saruhan, O. Freitag, P. Gazdzicki, T. Morawietz, R. Hiesgen, A. S. Gago, and K. A. Friedrich, "Low-cost and durable bipolar plates for proton exchange membrane electrolyzers," *Sci. Rep.*, vol. 7, no. March, pp. 1–12, 2017.

[46] A. S. Gago, S. A. Ansar, B. Saruhan, U. Schulz, P. Lettenmeier, N. A. Cañas, P. Gazdzicki, T. Morawietz, R. Hiesgen, J. Arnold, and K. A. Friedrich, "Protective coatings on stainless steel bipolar plates for proton exchange membrane (PEM) electrolysers," *J. Power Sources*, vol. 307, pp. 815–825, 2016.

[47] Tractebel and Hinicio, "Study on early business cases for H2 in energy storage and more broadly power to H2 applications," 2017.

[48] A. Nechache, M. Cassir, and A. Ringuedé, "Solid oxide electrolysis cell analysis by means of electrochemical impedance spectroscopy: A review," *J. Power Sources*, vol. 258, pp. 164–181, 2014.

[49] J. Wu, X. Z. Yuan, H. Wang, M. Blanco, J. J. Martin, and J. Zhang, "Diagnostic tools in PEM fuel cell research: Part I Electrochemical techniques," *Int. J. Hydrogen Energy*, vol. 33, no. 6, pp. 1735–1746, 2008.

[50] Metrohm, "Electrochemical Impedance Spectroscopy (EIS) Part 1 – Basic Principles," *Autolab Application Note EIS01*, pp. 1–3, 2011.

[51] S. Kolb, "Thermally Sprayed Low Cost Current Collectors with Optimized Mass Transport Behavior for PEM Electrolyzers," Stuttgart University, 2017.

[52] Berghoefer, "Aktuelle Tagespreise," 2018. [Online]. Available: http://www.berghoefer-metalle.de/service/metallpreise/. [Accessed: 19-Jun-2018].

[53] Edelmetalle, "Titanbarren 1kg (995 Ti)." [Online]. Available: http://www.edelmetall-handel.de/1kg-titanbarren-1000g.html. [Accessed: 19-Jun-2018].

[54] "Goodfellow." [Online]. Available: http://www.goodfellow.com/. [Accessed: 19-Jun-2018].

[55] Joint Research Centre, "EU Harmonised Polarisation Curve Test Method for Low Temperature Water Electrolysis." Publications Office of the European Union, Luxembourg:, p. 33, 2018.

[56] J. Yeh and I. Lindau, *Atomic subshell photoionization cross sections and asymmetry parameters: 1< Z> 103*, vol. 32, no. 1. Academic Press, 1985.

[57] J. Mo, S. M. Steen, F. Y. Zhang, T. J. Toops, M. P. Brady, and J. B. Green, "Electrochemical investigation of stainless steel corrosion in a proton exchange membrane electrolyzer cell," *Int. J. Hydrogen Energy*, vol. 40, no. 36, pp. 12506–12511, 2015.

[58] J. H. Van Der Merwe, "Characterisation of a proton exchange membrane electrolyser using electrochemical impedance spectroscopy," The School of Electrical, Electronic and Computer Engineering North-West University, 2012.

[59] C. Rozain and P. Millet, "Electrochemical characterization of Polymer Electrolyte Membrane Water Electrolysis Cells," *Electrochim. Acta*, vol. 131, pp. 160–167, 2014.
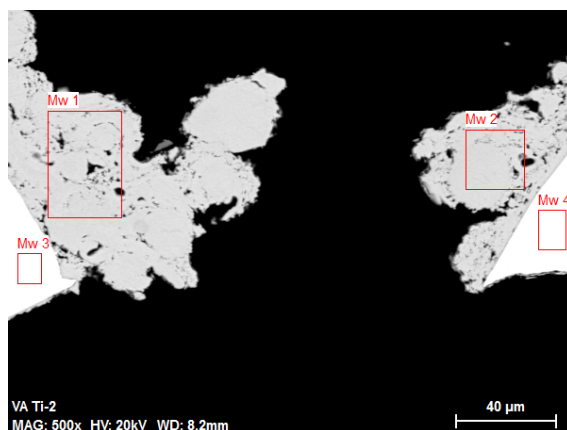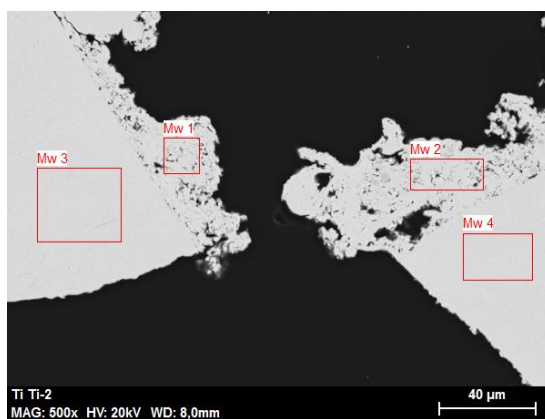
Appendix A

Figure 30 - EDX of a section of SS mesh/Ti.

Table 9 – Mass fraction of the elements in the areas described in **Figure 30** by EDX.

Area designation	Elements/ mf %							
	C	O	Si	Ti	Cr	Fe	Ni	Mo
Mw 1	0.00	-	-	100.00	-	-	-	-
Mw 2	0.00	-	-	100.00	-	-	-	-
Mw 3	0.00	0.72	0.37	0.43	17.03	43.10	10.83	2.20
Mw 4	0.00	0.81	0.41	0.38	16.96	21.9	9.80	2.43

Figure 31 - EDX of a section of Ti mesh/Ti.

Table 10 – Mass fraction of the elements in the areas described in **Figure 31** by EDX.

Area designation	Elements/ mf %
	Ti
Mw 1	100.00
Mw 2	100.00
Mw 3	100.00
Mw 4	100.00

Appendix B

Nyquist plots of the tested GDLs for 0.1, 0.5, 1.5 and 2 A·cm^{-2}.
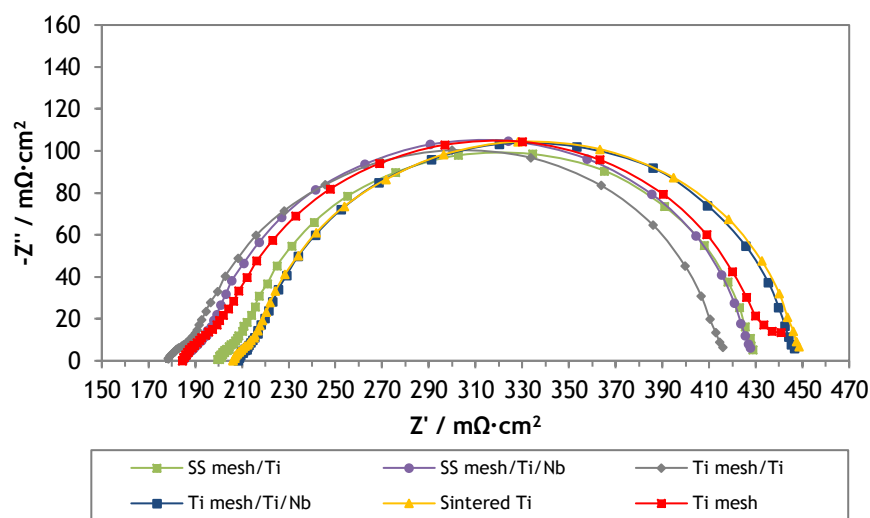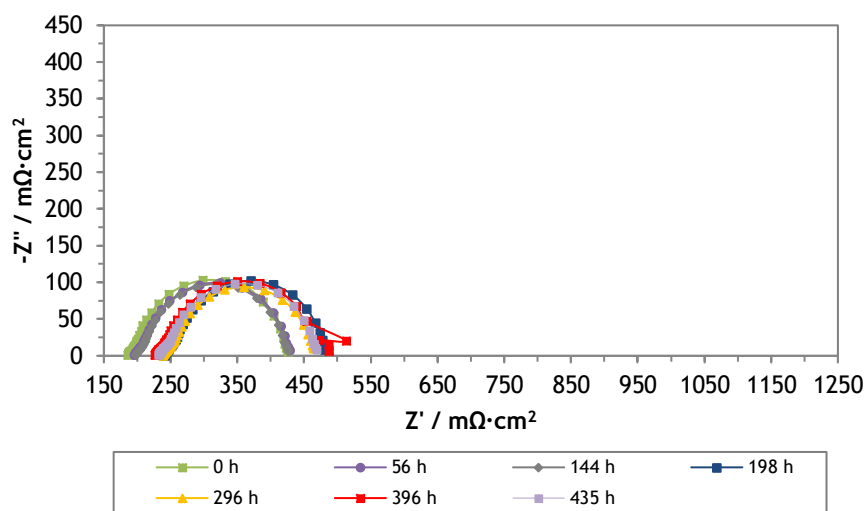

Figure 32 - Nyquist plots from the EIS measurements at 0.1 A·cm^{-2} (amplitude 50 mA). From 100 mHz to 50 kHz of frequency.
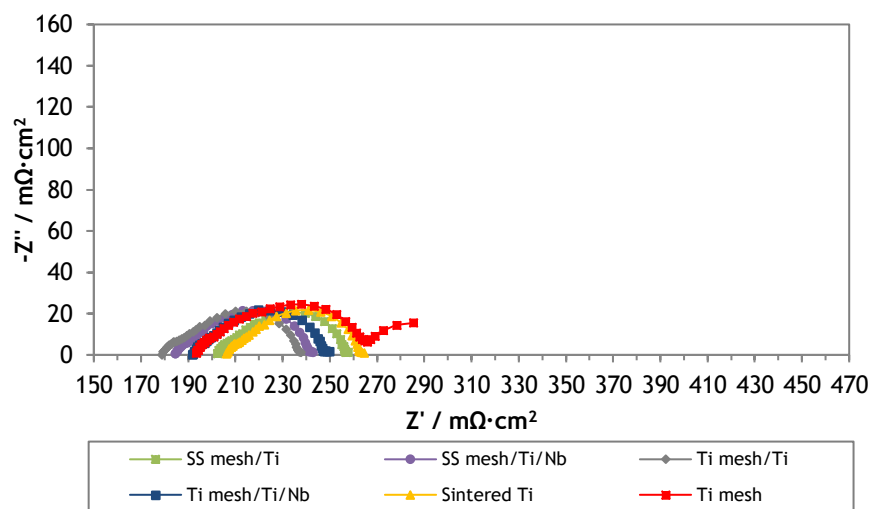
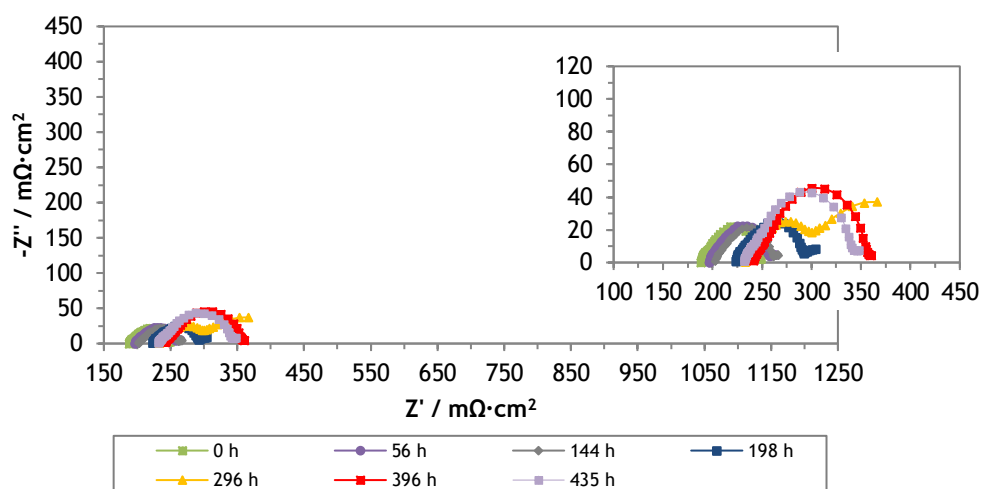Figure 33 - Nyquist plots from the EIS measurements at 0.5 A·cm^{-2} (amplitude 100 mA). From 100 mHz to 50 kHz of frequency.
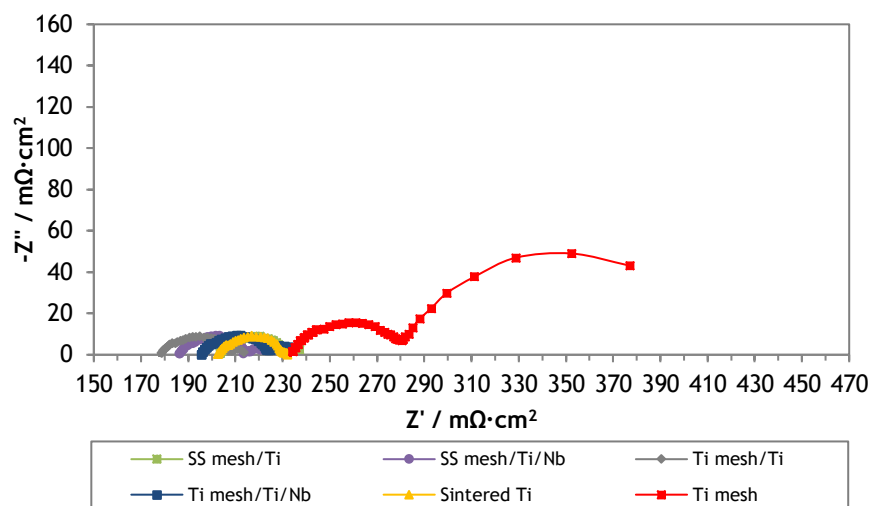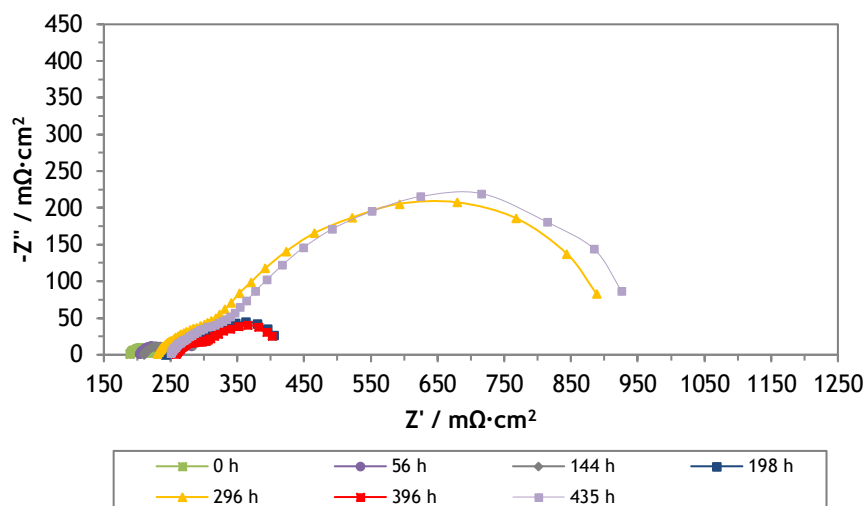
Figure 34 - Nyquist plots from the EIS measurements at 1.5 A·cm^{-2} (amplitude 200 mA). From 100 mHz to 50 kHz of frequency.
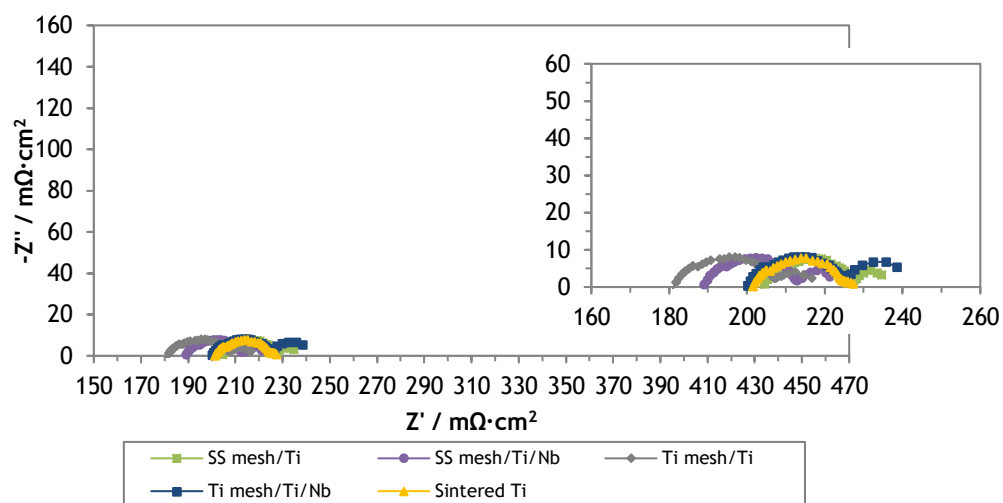
Figure 35 - Nyquist plots from the EIS measurements at 2 A·cm^{-2} (amplitude 200 mA). Ti mesh was not able to operate at this current density. From 100 mHz to 50 kHz of frequency.

Appendix C

Nyquist plots of log-term measurements of SS mesh/Ti/Nb for 0.1, 0.5, 1.5 and 2 A·cm^{-2}.

Figure 36 - Nyquist plots from the EIS long-term measurements of SS mesh/Ti/Nb at 0.1 A·cm^{-2} (amplitude 50 mA). From 100 mHz to 50 kHz of frequency.

Figure 37 - Nyquist plots from the EIS long-term measurements of SS mesh/Ti/Nb at 0.5 A·cm^{-2} (amplitude 100 mA). From 100 mHz to 50 kHz of frequency.
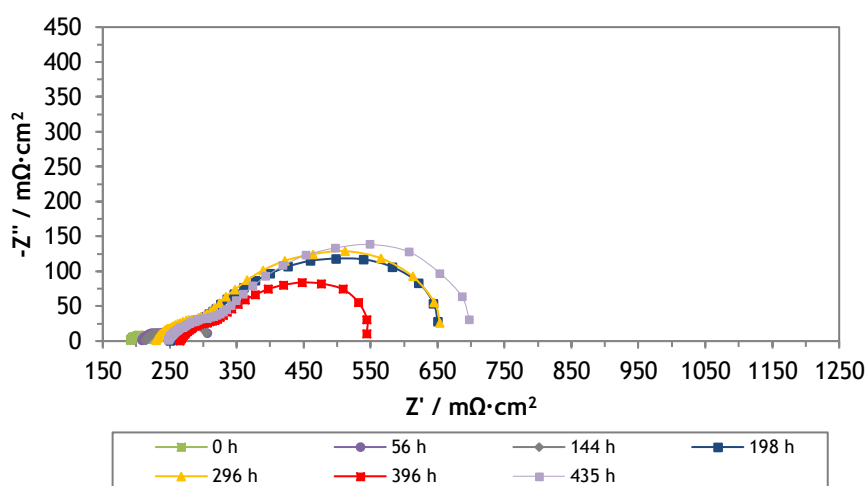
Figure 38 - Nyquist plots from the EIS long-term measurements of SS mesh/Ti/Nb at 1.5 A·cm^{-2} (amplitude 200 mA). From 100 mHz to 50 kHz of frequency.

Figure 39 - Nyquist plots from the EIS long-term measurements of SS mesh/Ti/Nb at 2 A·cm^{-2} (amplitude 200 mA). From 100 mHz to 50 kHz of frequency.
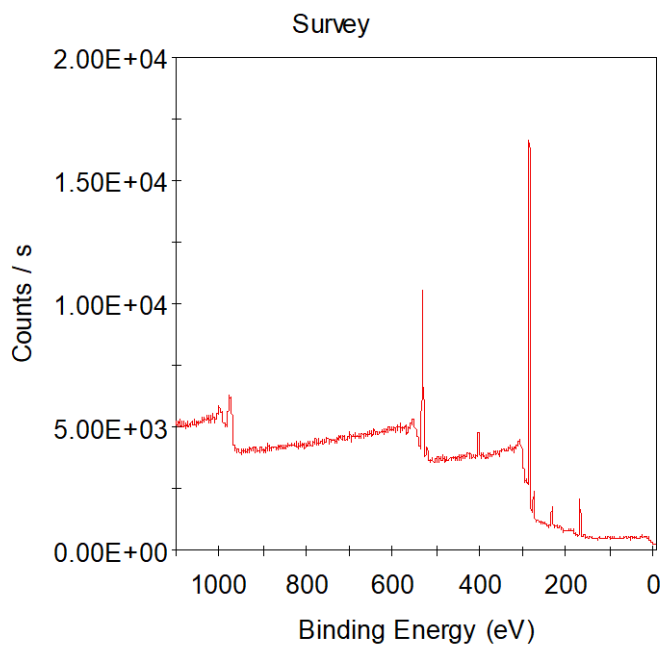
Appendix D

Figure 40 – XPS measurements for the pestle sample of DI water ion exchange resin. With base pressure of $5 \cdot 10^{-10}$ mbar with the energy resolution of 0.9 eV.
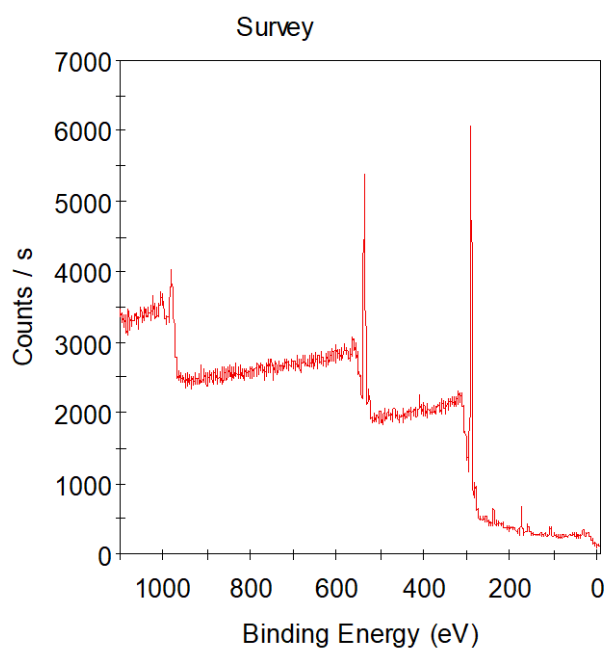

Figure 41 - XPS measurements for the not pestle sample of DI water ion exchange resin. With base pressure of $5 \cdot 10^{-10}$ mbar with the energy resolution of 0.9 eV.

Appendix E

Long-term measurements of 535 h of sintered titanium and titanium net in the anode GDL, with MEA E500 at 65 °C.
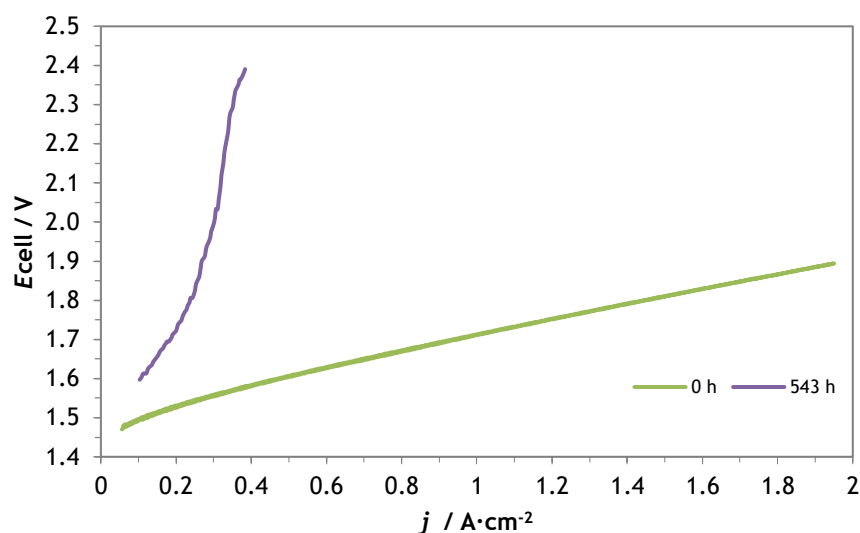

Figure 42 - Polarization curve of long-term measurement of sintered titanium with a titanium net in the anode side till 2 A·cm^{-2}, at 65 °C, atmospheric pressure and with an active area in the cell components of 4 cm^2.
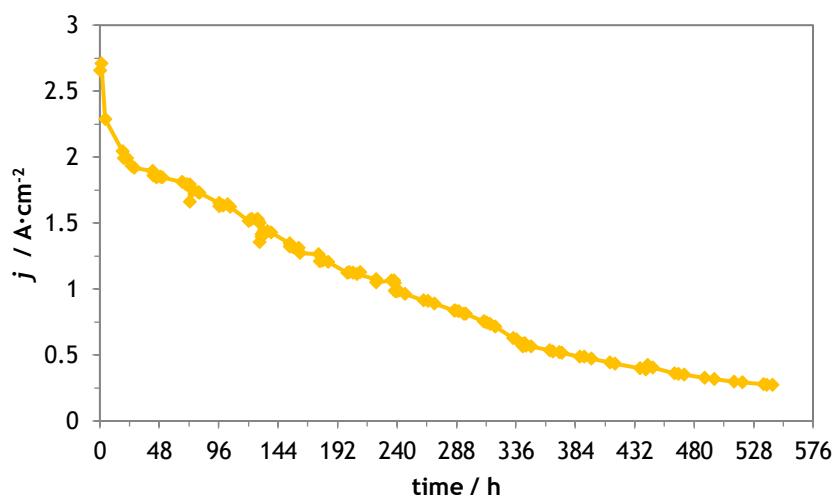

Figure 43 - Long-term testing of sintered titanium with a titanium net in the anode side at constant 2 V and 65 °C. The values of potential were recorded manually over the period of 543 h.